



# Εθνικό Μετσόβιο Πολυτεχνείο

Μεταπτυχιακή Διπλωματική Εργασία

---

Ανάπτυξη πιθανοτικών μοντέλων προσδιορισμού  
της μέγιστης αντοχής σε θλίψη ναυπηγικών  
ελασμάτων

---

Συγγραφέας:  
Στέφανος Ι. Καρράς

Επιβλέπων:  
Επίκουρος Καθ. Κ. Ν.  
Ανυφαντής

Η παρούσα εργασία εκπονήθηκε για την απόκτηση μεταπτυχιακού  
διπλώματος ειδίκευσης

στον

Τομέα Θαλασίων Κατασκευών  
Σχολή Ναυπηγών Μηχανολόγων Μηχανικών

Αθήνα, Ιανουάριος 2022





NATIONAL TECHNICAL UNIVERSITY OF  
ATHENS

MASTER THESIS

---

**Probabilistic modeling for buckling strength  
assessment of steel plates in ship hulls**

---

*Author:*  
Stefanos I. Karras

*Supervisor:*  
Assistant Prof. K. N.  
Anyfantis

*This dissertation is submitted for the degree of Master of Science  
in the*

Shipbuilding Technology Laboratory  
School of Naval Architecture and Marine Engineering

Athens, January 2022



## *Acknowledgements*

First and foremost, I want to thank my supervisor, Assistant Professor Konstantinos Anyfantis, for introducing me to new information and knowledge in both his seminars and our meetings. His ongoing assistance and encouragement, in addition to being an exceptional teacher, has been really beneficial and motivating.

In addition, I'd want to express my gratitude to all of my loved ones and friends, both old and new, who have emotionally supported me through difficult times and helped me grow as a person, both during my school years and during my college studies.

Finally, I'd like to express my gratitude to my family for their love, support, and encouragement.

I hope you find this effort to be up to your standards.



## *Abstract*

The compressive resistance of steel plates used in ship structures is studied from a reliability perspective in an attempt to generate probabilistic curves that may be used within the framework of risk-based design. Uncertainty in the material properties (elasticity and plasticity) and production-related geometric distortions have been probabilistically modeled by considering realistic statistical structures. For time efficiency, a pre-defined number of detailed non-linear finite element models have been constructed and simulated based on design of experiments (DOE) sampling schemes in accordance with the response surface methodology. The generated surrogates were first validated and then used within a Monte Carlo Simulation (MCS) framework for uncertainty propagation. The probabilistic resistance of the plate populations of interest was obtained by identifying a parametric statistical model based on the sample statistics. The obtained statistical structures allowed for the generalized reliability assessment of steel plates, which further enables the comparison with empirical formulations found in rules and in the scientific literature.





## Περίληψη

Η προτεινόμενη Μ.Ε. εντάσσεται στο πεδίο της μελέτης της δομικής αξιοπιστίας των επιμέρους κατασκευαστικών υποσυνόλων που απαρτίζουν την μεταλλική κατασκευή σκαφών και πιο συγκεκριμένα ναυπηγικών ελασμάτων που υπόκεινται σε θλιπτικά φορτία. Βασικός σκοπός της είναι η δημιουργία διαγραμμάτων λυγισμικής αντοχής συναρτήσει του βαθμού λυγηρότητας οι οποίες θα συνδέονται με μία καθορισμένη πιθανότητα αστοχίας. Η αβεβαιότητα στις ιδιότητες του υλικού (ελαστικότητα και πλαστικότητα), καθώς και οι αρχικές ατέλειες στην γεωμετρία που σχετίζονται με την παραγωγή, έχουν μοντελοποιηθεί πιθανοτικά λαμβάνοντας υπόψη ρεαλιστικές στατιστικές κατανομές. Όστε να επιτευχθεί η βέλτιστη χρονική απόδοση, ένας προκαθορισμένος αριθμός λεπτομερών μη γραμμικών μοντέλων πεπερασμένων στοιχείων έχει κατασκευαστεί και προσομοιωθεί με την εκπαίδευση στατιστικών μοντέλων παλινδρόμησης σύμφωνα με τη μεθοδολογία απόκρισης επιφάνειας. Οι εναλλακτικές εξισώσεις που δημιουργήθηκαν, αρχικά επικυρώθηκαν και στη συνέχεια, για την παραγωγή των τυχαίων μεταβλητών και τη διάδοση των αβεβαιοτήτων, πραγματοποιηθούν στατιστικές προσομοιώσεις Μόντε Κάρλο. Τα ληφθέντα στατιστικά μοντέλα επέτρεψαν τη γενικευμένη αξιολόγηση αξιοπιστίας των ναυπηγικών ελασμάτων, τα οποία επιτρέπουν περαιτέρω τη σύγκριση με εμπειρικές συνθέσεις που βρίσκονται στους κανονισμούς και στην επιστημονική βιβλιογραφία.



# Contents

<b>Acknowledgements</b>	<b>iii</b>
<b>Abstract</b>	<b>v</b>
<b>1 Introduction</b>	<b>1</b>
<b>2 Fundamental Theory of Plate Buckling</b>	<b>3</b>
2.1 Plate Buckling . . . . .	3
2.2 General Framework . . . . .	6
2.3 Empirical Formulations . . . . .	10
<b>3 Uncertainty Definition</b>	<b>11</b>
3.1 Uncertainty Associated with the Design Variables . . . . .	11
3.2 Uncertainty Definition of Design Variables . . . . .	12
3.2.1 Uncertainty in Initial Imperfection . . . . .	12
3.2.2 Uncertainty in Material Properties . . . . .	14
<b>4 Finite Element Method</b>	<b>17</b>
4.1 Nonlinear Finite Element Analysis . . . . .	19
4.1.1 Material Nonlinearity . . . . .	19
4.1.2 Linear Elastic Material Model . . . . .	21
4.1.3 Bilinear Material Model . . . . .	21
4.1.4 Nonlinear Solution . . . . .	22
4.2 Finite Element Modeling . . . . .	22
4.2.1 Material Model . . . . .	22
4.2.2 Element Type & Size . . . . .	23
4.2.3 Geometrical Initial Imperfections . . . . .	24
4.2.4 Boundary & Loading Conditions . . . . .	24
4.2.5 FE Model Validation . . . . .	25
<b>5 Probabilistic Modeling</b>	<b>27</b>
5.1 Monte Carlo Simulation . . . . .	27
5.2 Surrogate Modeling . . . . .	28
5.2.1 Design of Experiments . . . . .	28
5.2.2 Response Surface Methodology . . . . .	28
<b>6 Results - Discussion</b>	<b>31</b>
6.1 RSM Results . . . . .	31
6.2 MCS Results . . . . .	31
6.3 Probabilistic Buckling Curves . . . . .	34

6.4 Proposed Safety Factors (PSFs) . . . . .	36
<b>7 Conclusions</b>	<b>37</b>
<b>Bibliography</b>	<b>39</b>
<b>A Matlab Source Code</b>	<b>41</b>
<b>B Ansys Source Code</b>	<b>49</b>

# List of Figures

2.1	Buckling mechanism of a rectangular plate. . . . .	3
2.2	Rectangular plate under uni-axial compression. . . . .	4
2.3	Buckling mode shape of rectangular plate. . . . .	5
2.4	Buckling coefficient for different aspect ratios $\alpha = a/b$ . . . . .	6
2.5	Buckling modes for aspect ratios of $\alpha = 2, 3, 4, 5$ . . . . .	7
2.6	Illustration of a plate found on a ship's deck. . . . .	8
3.1	Statistical structure of a plate's initial deflection. . . . .	13
3.2	Probability distribution of steel S235 yield strength. . . . .	15
3.3	Probability distribution of Young's elastic modulus of steel S235. . . . .	15
4.1	Load-displacement relationship for an elastic spring structure. . . . .	18
4.2	Linear and nonlinear structural response. . . . .	20
4.3	Typical stress-strain curve for structural steel. . . . .	20
4.4	Elastic-perfectly plastic material. . . . .	21
4.5	Bilinear material. . . . .	21
4.6	Schematic of the Newton-Raphson method. . . . .	22
4.7	Geometry demonstrations of a 4-node (A) and a 8-node (B) element. . . . .	23
4.8	Mesh convergence study. . . . .	24
4.9	Plate's boundary and loading conditions. . . . .	25
4.10	Phases of plastic strain (A) and von Misses stress (B). . . . .	26
5.1	Illustration of faced central composite design sampling for surrogate modeling. (Figure borrowed from Matlab documentation. . . . .	29
6.1	Statistical analysis of normalized resistance with the aid of a histogram (A) and a Q-Q plot (B). . . . .	32
6.2	Latin Hypercube sampling for MCS visualized through pairs of RVs. . . . .	33
6.3	Probabilistic resistance curves (buckling curves). . . . .	35
6.4	Probability of failure for each empirical model per slenderness ratio. . . . .	35
6.5	Explanation of Eq. 6.3 (Rahman et al., 2017). . . . .	36



# List of Tables

2.1	List of plate dimensions. . . . .	9
5.1	Experiment matrix for surrogate modeling generation through FE simulations. . . . .	29
6.1	Coefficients of the RS obtained from the finite elements simulation.	34





# Chapter 1

## Introduction

The majority of marine structures are constructed from slender platings that are stiffened in both longitudinal and transverse directions. They are seen as thin-walled structures, and their analysis and design are therefore based on assumptions and considerations related to such structures. Hull girder bending loads introduce primary bending stresses to the vessel, which tend to extend or compress the stiffened panels that constitute the construction. During the hull scantling design process, each plate element (unsupported area between stiffeners) needs to be assessed against its local buckling collapse mode. Class rules involve empirical formulations for buckling strength assessment and there is on-going research towards deriving new, more accurate formulas by employing Finite Element simulations, sometimes combined with experiments.

For many years, a significant amount of research has been directed towards experimental modelling of different ship structural elements, as well as towards the development of analytical and numerical methods to improve their design against buckling. For example, Chryssanthopoulos, 1998 reviewed probabilistic concepts and their application to thin-walled plates and shells susceptible to buckling failure, while Ivanov, 2013 focused on the hull girder reliability and Rahman et al., 2017; Rahman et al., 2020 on the ultimate buckling strength of stiffened steel plates.

The proposed work focuses on a probabilistic strength approach to plate compression. The main objective is to obtain buckling curves as a function of the plate's slenderness ratio that are correlated with a defined probability of failure. This action will allow for comparing the reliability of the empirical formulae found in rules and for the probabilistic buckling analysis of plates. Quantified uncertainty was considered for geometric initial imperfections and for the material's elastoplastic parameters. Surrogate models based on non-linear finite element simulations have been generated and fed into a MCS for uncertainty propagation. The parametric statistical structures of the plate's resistance allowed for the derivation of probabilities of failure that were interpolated over the slenderness ratio range of interest. This allowed for the derivation of probabilistic buckling resistance curves.



## Chapter 2

# Fundamental Theory of Plate Buckling

### 2.1 Plate Buckling

The rigidity of the surrounding stiffeners has a big impact on the support at the plating edges. The plate is considered to be simply supported at all edges in this proposed work because this results in the least critical stress and is thus a safe assumption. The load is applied on the plate's short edge (breadth). Ideal plates are subject to elastic buckling. An ideal plate is one with a constant thickness ( $t$ ), is formed of linear elastic material with no residual stresses, and is loaded exactly in the mid-plane (Hughes and Paik, 2010).

Figure 2.1 depicts the buckling mechanism of a rectangular plate. At first, the applied load is lower than the critical one, and the out of plane deflection is small, when the applied load reaches the critical value. Following this, the plate buckles, forming one half wave across its length and breadth. At this point, the fibers in the direction of compression have shortened while the fibers perpendicular to the stress direction lengthen. The transverse strips not only support the longitudinal strips against buckling but also contribute to a further increase in strength capacity (postbuckling strength). It should be noted that the breadth of the plate is strongly related to the critical buckling stress; the increase in breadth leads to decreased critical stress. This can be explained by the fact that the increase in breadth leads to decreased slopes

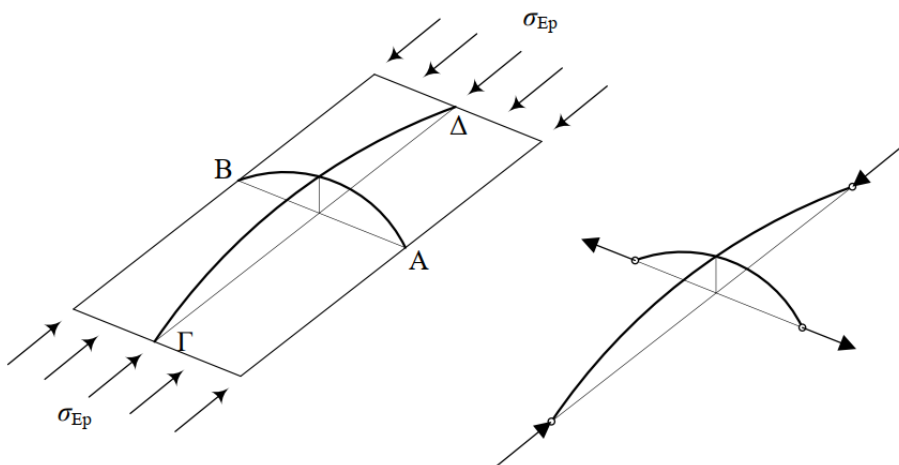


FIGURE 2.1: Buckling mechanism of a rectangular plate.

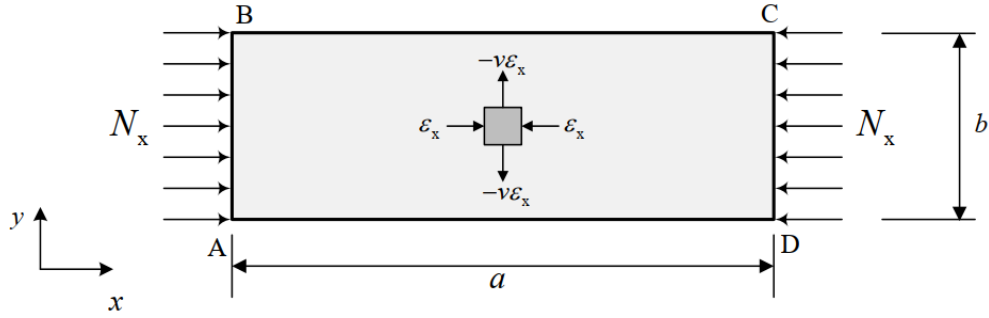


FIGURE 2.2: Rectangular plate under uni-axial compression.

of the transverse strips, and under these circumstances, the maximum out-of-plane deflection decreases.

Next, the buckling stress of a rectangular plate such as the one shown in Figure 2.2 is calculated. Assuming that the coordinate system  $(x,y)$  uses  $x$  in the long direction and  $y$  in the short direction, the plate dimensions of the plate are  $a$  in length,  $b$  in width, and  $t$  in thickness.

Considering the situation where bending has occurred and the plate has acquired a bending arrow with respect to the two axes of the plane, the partial differential equation describing the problem is given as:

$$D \left\{ \frac{\partial^4 w}{\partial x^4} + 2 \frac{\partial^4 w}{\partial x^2 \partial y^2} + \frac{\partial^4 w}{\partial y^4} \right\} + N_x \frac{\partial^2 w}{\partial x^2} = 0, \quad (2.1)$$

where  $w$  is the deflection and  $D$  is the flexural rigidity, computed from the following equation:

$$D = \frac{Et^3}{12(1-\nu^2)}, \quad (2.2)$$

The calculation of buckling stress for plates is an eigenvalue problem like the buckling of perfect columns. The solution of the above differential equation is the product of two harmonic functions:

$$w = \sin\left(\frac{m\pi x}{a}\right) \sin\left(\frac{n\pi y}{b}\right), \quad (2.3)$$

The parameters  $m$  and  $n$  indicate the number of half waves in each direction of the buckled shape.  $m$  is the number of half waves along the long edge ( $x$ -axis) of the plate, while  $n$  is the number of half waves along the plate's short edge ( $y$ -axis). Figure 2.3 depicts a rectangular plate with three half-waves along the long edge and one half wave along the short edge.

The eigenvalues of the partial differential equation are calculated as:

$$N_{m,n} = D \left( \frac{\pi a}{m} \right)^2 \left[ \left( \frac{m}{a} \right)^2 + \left( \frac{n}{b} \right)^2 \right]^2, \quad (2.4)$$

For every eigenvalue, the deflected shape of the plate (mode shape) can be calculated from Eq. (2.2)

Note that the smallest value of  $N$  for all values of  $a$ ,  $b$  and  $m$  is obtained if  $n = 1$ . This means that only one half wave will be formed in the direction perpendicular to

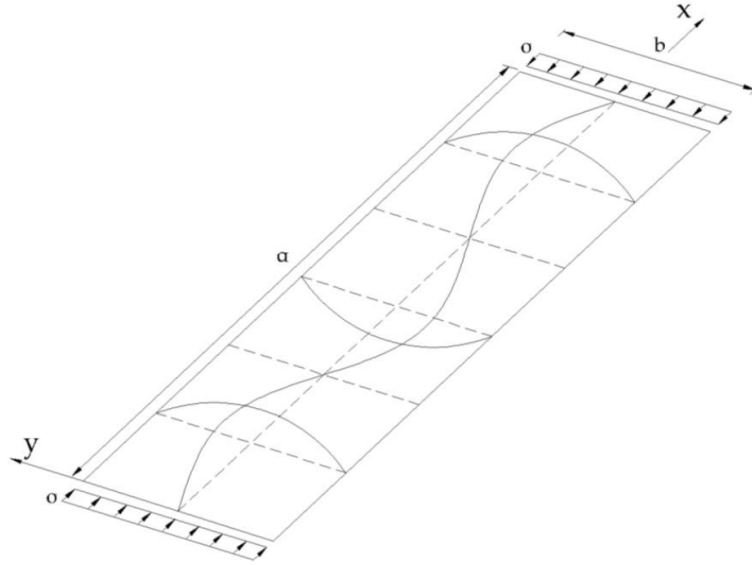


FIGURE 2.3: Buckling mode shape of rectangular plate.

the load application. Then, it can be written as a simple form:

$$N_m = \left( \frac{mb}{a} + \frac{a}{mb} \right)^2 \frac{D\pi^2}{b^2}, \quad (2.5)$$

Substituting Eq. (2.2) into Eq. (2.5), setting  $\alpha = a/b$  and  $\sigma_{Ep} = N_m/t$  the elastic buckling stress formula which is also known as the Bryan formula, is obtained:

$$\sigma_{Ep} = K_c \frac{\pi^2 E}{12(1-\nu^2)} \left( \frac{t}{b} \right)^2, \quad (2.6)$$

where  $K_c$  is the critical buckling coefficient. The expression for the buckling coefficient  $K$  depends on the type of boundary support as well as the loading type. For simply supported plates under uniaxial compression in the  $x$ -direction,  $K$  is given by:

$$K = \left( \frac{m}{a} + \frac{a}{m} \right)^2, \quad (2.7)$$

The buckling half wave number  $m$  can be determined as the minimum integer satisfying the following inequality:

$$\frac{a}{b} \leq \sqrt{m(m+1)}, \quad (2.8)$$

Figure 2.4 shows the buckling coefficient  $K$  plotted against aspect ratio  $a/b$  for various values of  $m$ . In Figure 2.4 it is also shown that the critical value of  $\sigma_{Ep}$  will occur for different values of  $m$  depending on the aspect ratio. It can also be seen that  $K$  equals to 4 if the aspect ratio is an integer and that it approaches 4 as the aspect ratio increases. In realistic design,  $K=4$  is usually applied for panels because it leads to the minimum buckling stress.

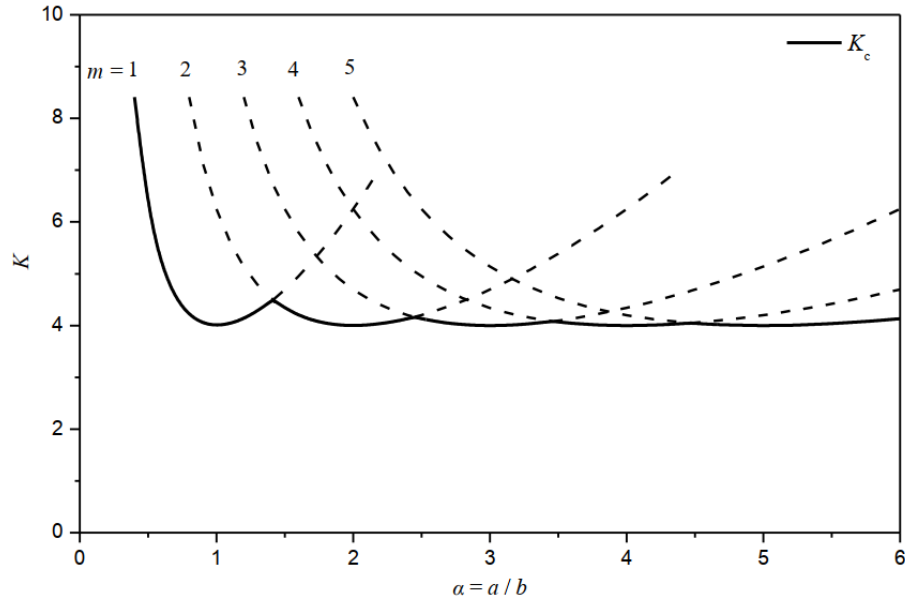


FIGURE 2.4: Buckling coefficient for different aspect ratios  $\alpha = a/b$ .

## 2.2 General Framework

The mid-ship region of a ship, e.g., of an oil tanker, can be regarded as a rectangular box encompassed by closely spaced longitudinal stiffeners and relatively widely spaced transverse frames. An illustration of the above can be visualised in Figure 2.6.

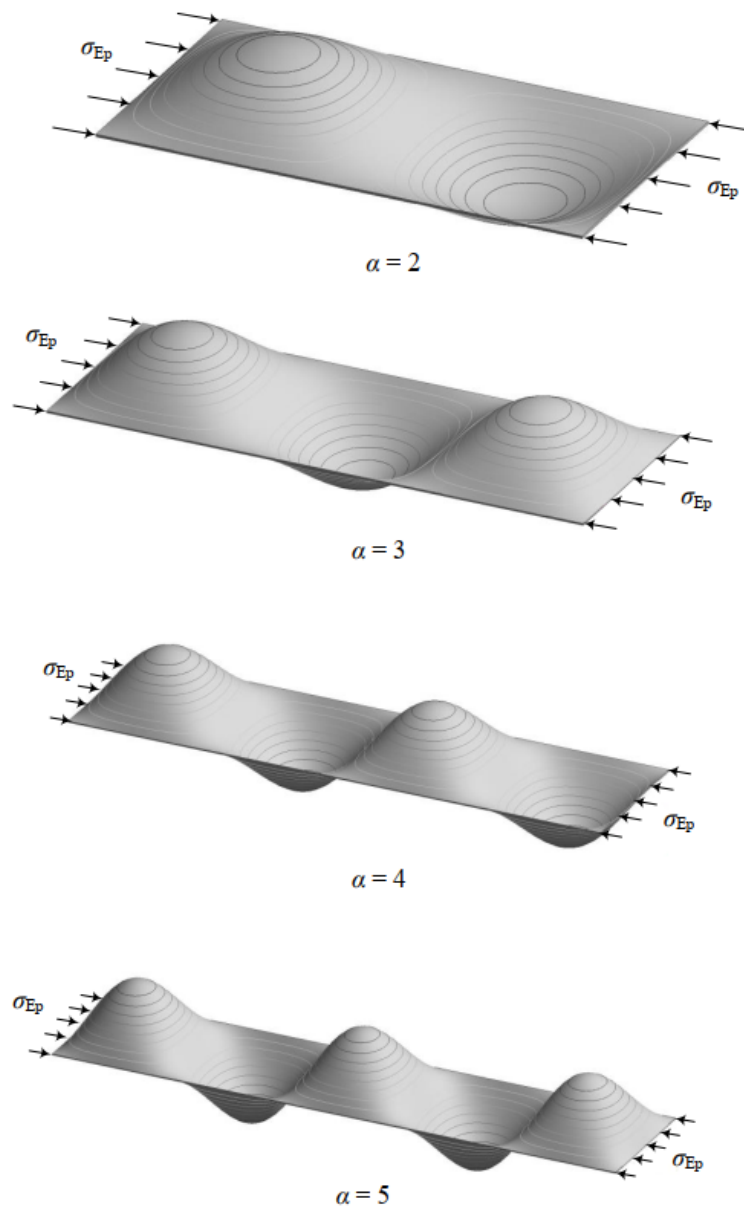
The scantlings of a plate hugely contribute to its mechanical behavior. According to Zhang, 2016, the typical value of the plating's aspect ratio,  $a/b$ , between stiffeners and transverse frames is 3.5–6.7 at the deck and bottom of the mid-ship regions. The length of  $a$  is in the range of 2.5–6.0 m and the width of  $b$  is in the range of 0.7–1.0 m. The width and thickness ratio of plating,  $b/t$ , is between 25 and 75. The thickness of the plating  $t$  is in the range of 12–36 mm. Buckling and ultimate strength are strongly related to a physical parameter called the plate slenderness ratio, and it is defined as follows:

$$\beta = \frac{b}{t} \sqrt{\frac{\sigma_y}{E}}, \quad (2.9)$$

where  $\sigma_y$  is the yield stress and  $E$  the Young's modulus. Values of  $\beta$  are typically in the range of 1.0 and 2.5.

For the purpose of the proposed work, 10 plate cases have been selected per slenderness ratio ( $\beta=1$ ,  $\beta=1.75$  and  $\beta=2.5$ ) resulting in 30 total plate cases that follow the scantlings' criteria mentioned above. Table 2.1 shows all 30 plate cases dimensions.

The considered model is a simply supported long plate subjected to axial loads acting at its short edges. This can represent the deck plating of a ship under vertical bending moments.

FIGURE 2.5: Buckling modes for aspect ratios of  $\alpha = 2, 3, 4, 5$ .

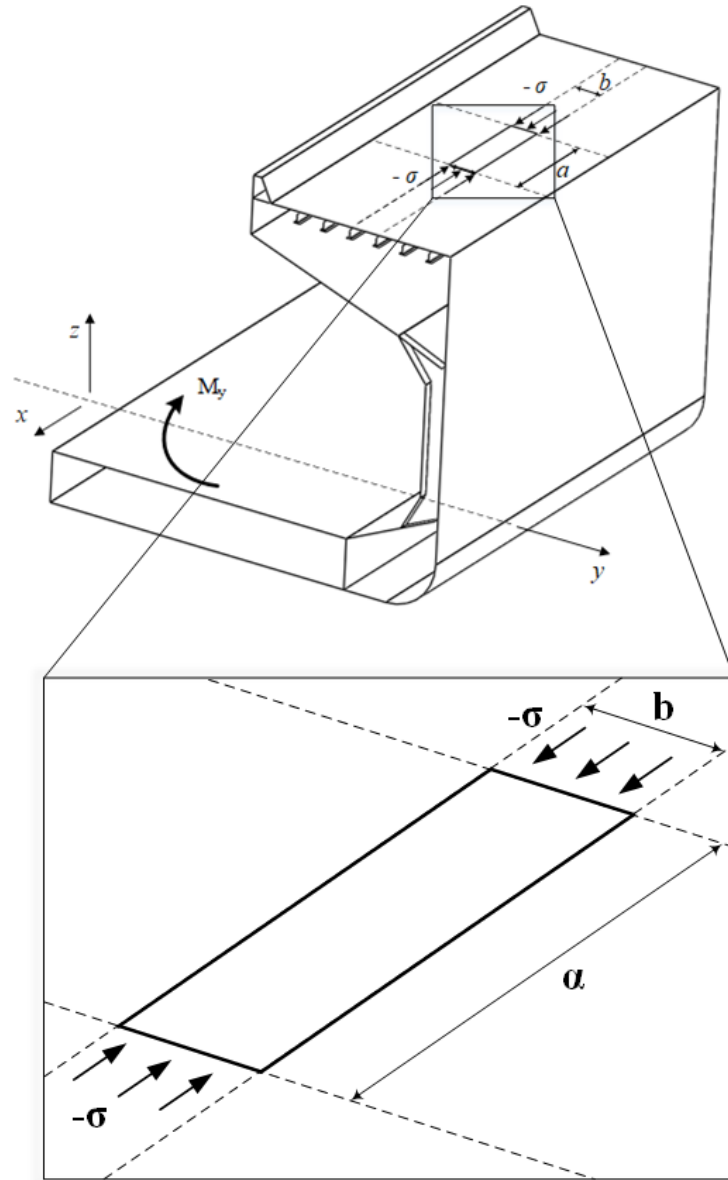


FIGURE 2.6: Illustration of a plate found on a ship's deck.



TABLE 2.1: List of plate dimensions.

Plate Slenderness ( $\beta$ )	Plate Series	b[mm]	t[mm]	b/t
1	1	718	24	29.92
	2	748	25	29.92
	3	778	26	29.92
	4	807	27	29.89
	5	837	28	29.89
	6	867	29	29.90
	7	896	30	29.87
	8	926	31	29.87
	9	956	32	29.88
	10	986	33	29.88
1.75	1	732	14	52.29
	2	786	15	52.40
	3	835	16	52.19
	4	839	16	52.44
	5	887	17	52.18
	6	891	17	52.41
	7	939	18	52.17
	8	944	18	52.44
	9	992	19	52.21
	10	996	19	52.42
2.5	1	894	12	74.50
	2	896	12	74.67
	3	898	12	74.83
	4	899	12	74.92
	5	900	12	75.00
	6	968	13	74.46
	7	969	13	74.54
	8	971	13	74.69
	9	973	13	74.85
	10	975	13	75.00

## 2.3 Empirical Formulations

Due to the complicated nature and non-linearity of the subject, it is difficult to seek analytical solutions for assessing the ultimate strength of plates. Therefore, semi-analytical and empirical approaches have been established over the years for developing design equations. Useful formulations have been developed, and some of these are listed below:

- Box, 1883:

$$\frac{\sigma_u}{\sigma_y} = \frac{1}{\beta^{0.5}}, \quad (2.10)$$

- Karman, 1924:

$$\frac{\sigma_u}{\sigma_y} = \frac{1.9}{\beta}, \quad (2.11)$$

- Schnadel, 1930:

$$\frac{\sigma_u}{\sigma_y} = 0.5 + \frac{1.81}{\beta^2}, \quad (2.12)$$

- Frankland, 1940:

$$\frac{\sigma_u}{\sigma_y} = \frac{2.25}{\beta} - \frac{1.25}{\beta^2}, \quad (2.13)$$

- Faulkner, 1975:

$$\frac{\sigma_u}{\sigma_y} = \frac{2}{\beta} - \frac{1}{\beta^2}, \quad (2.14)$$

It is worth noting that Faulkner's equation shows good agreement with extensive experimental data and has been widely accepted and used in the industry. It could also be noted that Frankland's equation, with only a marginal difference from Faulkner's method, was used by the US Navy and the International Association of Classification Societies (IACS) in the definition of the effective width of the attached plate in a stiffened structural element (IACS, 2021a).

## Chapter 3

# Uncertainty Definition

### 3.1 Uncertainty Associated with the Design Variables

As for all materials, there is a certain degree of randomness or uncertainty in our ability to predict both the loads imposed on the ship's structure (the demand) and the ability of the structure to withstand those loads (the capability). The sources of these uncertainties include phenomena that can be measured and quantified but cannot be perfectly controlled or predicted by the designer and phenomena for which adequate knowledge is lacking. The term "objective uncertainties" is sometimes applied to describe the former, and the term "subjective" is used to describe the latter. In principle, the objective uncertainties can be expressed in statistical terms using available data and theoretical procedures. The subjective uncertainties, which are known to exist but which cannot be quantified as a result of a lack of knowledge, must be dealt with through judgment and the application of factors of safety.

An example of an objective uncertainty is the variability in the strength properties of the steel used in constructing a ship. The magnitude of this variability is controlled to some extent through the practices of specifying minimum properties for the steel and testing the material as produced by the steel mill to ensure compliance with the specifications. Departures from the specified properties may exist for several reasons. For practical reasons, the sampling and testing cannot be applied to all of the material going into the ship, but only to a limited sampling of the material. As a result of slight variations in its manufacturing experience, some of the material may exhibit different properties from those of material manufactured by supposedly identical procedures. After arrival in the shipyard, the material properties may be altered by the operations such as cutting, forming, and welding, which are involved in building it into the ship. These variations in properties may be reduced by a more rigorous system of testing and quality control, all of which adds to the final cost of the ship. A compromise must therefore be reached between cost and the level of variation or uncertainty that is considered acceptable and that may be accommodated by the degree of conservatism in the design.

On the other hand, the subjective uncertainty cannot be quantified on the basis of direct observation or analytical reasoning but must be deduced by indirect means. The most common source of this uncertainty is a deficiency in the understanding of a fundamental physical phenomenon or an incomplete development of the mathematical procedures needed for the purpose of predicting a certain aspect of the structural response. Even though there have been important advances in theoretical and computational methods of nonlinear structural analysis, there is still a significant element of uncertainty in predictions of structural behavior in the vicinity of structural collapse.

In this region, nonlinear material behavior as well as nonlinear geometric effects are present, and the overall response may involve the sequential interaction of several elementary response phenomena. Of course, it is the goal of ongoing research to change these subjective uncertainties into objective uncertainties.

Therefore, it is clear that the design of ship structures must take into account the uncertainties in the predictions of both demand and strength. To arrive at the most efficient structure that will achieve an acceptable degree of reliability, it is necessary to attempt to quantify the uncertainties and allow for their possible magnitudes and consequences. Reliability assessment offers an excellent means for doing this.

The direct integration method of reliability analysis can be difficult to apply in practice. The two main reasons for this are the lack of information to determine the joint probability density function (JPDF) of the design variables and the difficulty associated with the evaluation of the resulting multiple integral. For these reasons, approximate methods of reliability analysis were developed. These methods are:

- Mean value first order second moment method (MVFOSM)
- First order reliability methods (FORM)
- Second order reliability methods (SORM)
- Advanced mean value method (AMV)
- Adaptive importance sampling (AIS)
- Monte Carlo simulation (MCS)

## 3.2 Uncertainty Definition of Design Variables

The compressive strength or resistance of a plate depends on geometrical and material parameters, which in reality are not deterministic quantities but differ from part to part as a result of production and assembly related processes. Within a structural reliability framework, these may be considered as uncertainties that obey a given statistical structure. In this direction, the Young's modulus ( $E$ ), the yield stress ( $\sigma_y$ ) and the initial bow imperfection ( $w_o$ ) were considered as Random Variables (RVs). Therefore, the plate's resistance may be expressed in probabilistic terms through the uncertainty propagation of the input parameters.

### 3.2.1 Uncertainty in Initial Imperfection

According to the International Association of Classification Societies (IACS, 2021b), typical values of accepted fairness of plating between frames in a strength deck are allowed to be a maximum of 4 mm at standard operating conditions, with 8 mm being the upper allowable limit. Also, according to experimental studies, the initial deflection follows the lognormal distribution (Dou and Pi, 2016), having the following

functional form:

$$f(w_o) = \begin{cases} \frac{1}{w_o \sqrt{2\pi}\sigma} \exp\left[-\frac{1}{2} \left(\frac{\ln w_o - \mu}{\sigma}\right)^2\right], & w_o \geq 0 \\ 0, & w_o < 0 \end{cases} \quad (3.1)$$

where the mean value  $m$  and variance  $\nu$  are a function of the parameters  $\mu$  and  $\sigma$  as follows:

$$\begin{aligned} m &= \exp\left(\mu + \frac{\sigma^2}{2}\right), \\ \nu &= \exp(2\mu + \sigma^2)[\exp(\sigma^2) - 1], \end{aligned} \quad (3.2)$$

For the estimation of a plate's resistance, without loss of generality and according to the above, the shape of the distribution derives from the following assumptions: In 85% of the observations, the initial plate deflection is less than 4 mm, and in 99% of the cases, the initial deflection is less than 8 mm. The values of the parameters can be retrieved from the following system of equations:

$$\begin{cases} F(w_o = 4) = \Phi\left(\frac{\ln 4 - \mu}{\sigma}\right) = 0.85 \\ F(w_o = 8) = \Phi\left(\frac{\ln 8 - \mu}{\sigma}\right) = 0.99 \end{cases} \quad (3.3)$$

where  $\Phi$  is the cumulative distribution function of the standard normal distribution (i.e.,  $N(0,1)$ ). Therefore, the initial plate deflection shall follow the lognormal distribution as given in Figure 3.1.

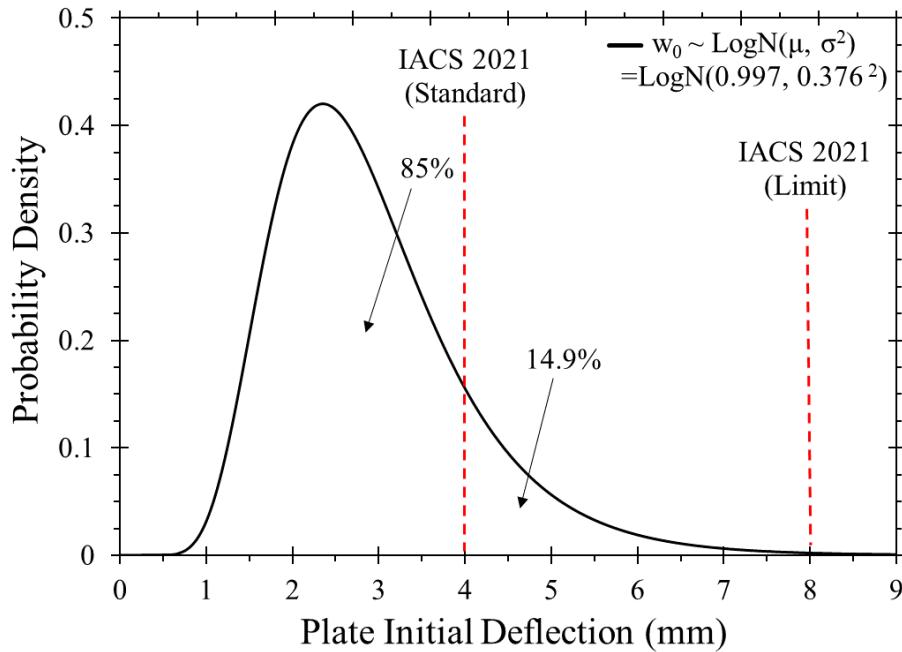


FIGURE 3.1: Statistical structure of a plate's initial deflection.

### 3.2.2 Uncertainty in Material Properties

According to experimental results for grade A steel (with a nominal yield stress equal to 235 MPa), the yield strength may follow a normal or lognormal distribution, with a mean value of 284.5 MPa and a standard deviation of 21.5 MPa (Melcher et al., 2004). To account for the fact that yield stress takes only positive values, the lognormal distribution was used instead, which follows Eq. (3.4). Given the mean value  $m$  and standard deviation  $\nu$ , the lognormal distribution parameters  $\mu$  and  $\sigma$  can be calculated through statistics. As a result, the parameters of the probability density function representing the yield strength distribution are  $\mu = 5.648$  and  $\sigma = 0.076$ . An illustration of the above can be seen in Figure 3.2.

$$f(\sigma_y) = \begin{cases} \frac{1}{\sigma_y \sqrt{2\pi}\sigma} \exp\left[-\frac{1}{2}\left(\frac{\ln \sigma_y - \mu}{\sigma}\right)^2\right], & \sigma_y \geq 0 \\ 0, & \sigma_y < 0 \end{cases} \quad (3.4)$$

Furthermore, the Young's elastic modulus of steel grade S235 may follow the normal distribution, with a mean value of  $\mu = 210$  GPa and a standard deviation of  $\sigma = 12.6$  GPa (Kala, 2007). The probability density function of the elastic modulus is given by:

$$f(E) = \frac{1}{\sqrt{2\pi}\sigma} e^{-\frac{1}{2}\left(\frac{E-\mu}{\sigma}\right)^2}, \quad -\infty < E < +\infty \quad (3.5)$$

and its statistical structure is shown in Figure 3.3.

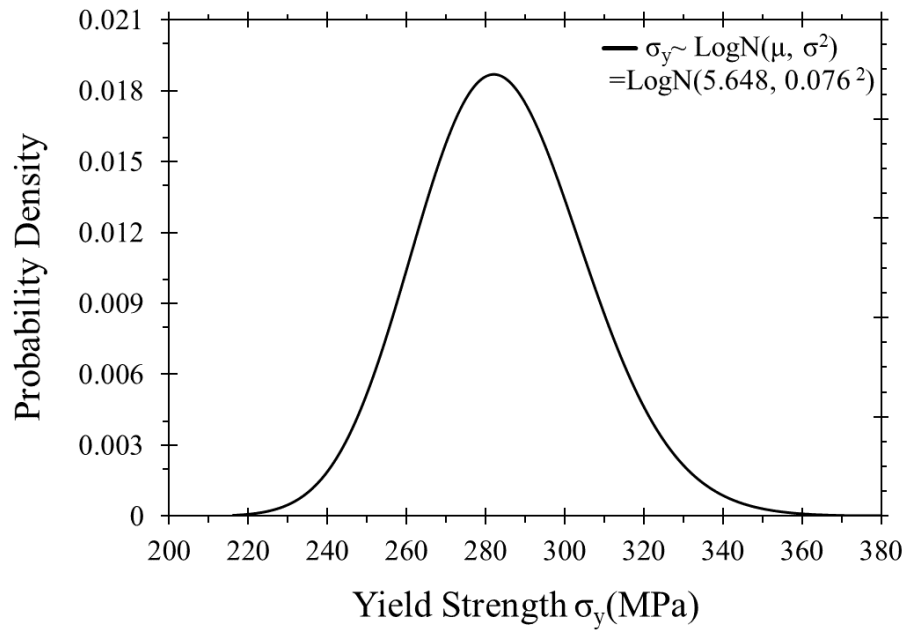


FIGURE 3.2: Probability distribution of steel S235 yield strength.

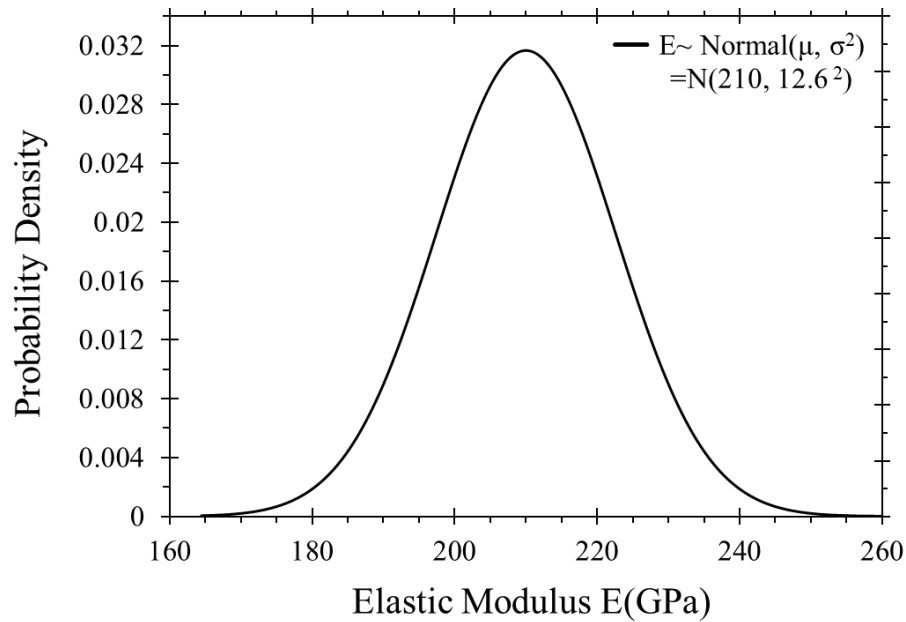


FIGURE 3.3: Probability distribution of Young's elastic modulus of steel S235.





## Chapter 4

# Finite Element Method

Finite element analyses have proven to be adequate for modeling initial distortions in stiffened panels. In this chapter, the fundamentals of the Finite Element Method (FEM) are discussed, and the stiffness matrix is derived. It is assumed that the external forces acting on the element are known and that the nodal displacements are unknown.

The discretization of a continuum and its representation as an assemblage of individual structural components, interconnected at a definite number of nodes, is the fundamental concept of finite element analysis. The structure's artificial elements are commonly triangles or quadrilaterals, with nodes at the corners. Regardless of the number of finite components used, a discrete model will not be able to produce an exact description of a continuous structure. Although the correctness of the solution improves as the number of elements employed grows, utilizing a large number of elements increases the calculation time. By carefully identifying and specifying the element attributes, the goal is to minimise the error rate. As a result, careful subdivision and selection of functions defining displacements and stresses inside and between parts is required.

The structure must be expressed in terms of a finite number of discrete variables in order to employ matrix methods. The nodal displacements and their derivatives are the variables in question. The nodal displacements must be connected to the internal displacements of the elements as well as their interactions. The nodal displacements are then the sole unknowns, and the problem is discrete rather than continuous. Despite the huge number of nodal displacements, there are only a finite number of discrete variables that are interconnected by linear equations and can be handled using matrix methods. The equations of equilibrium and geometric compatibility must be satisfied everywhere, both inside and between the elements, in order to produce accurate solutions.

The device most directly associated with stiffness is a simple elastic spring that undergoes axial displacements and transmits axial forces. The following formula is used to calculate the force caused by the imposed displacement and vice-versa.

$$F = KU, \quad (4.1)$$

where  $F$  is the internal force,  $K$  is the stiffness of the spring and  $U$  is the internal deformation. The same spring can be regarded as a whole structure, the load causes a structure displacement  $U$  which is proportional to  $F$  and the constant of proportionality  $K$  is termed as the structure's stiffness.

Knowing the stiffness and the applied load Eq. 4.1 may be inverted to give the displacement.

$$U = \frac{1}{K}F, \quad (4.2)$$

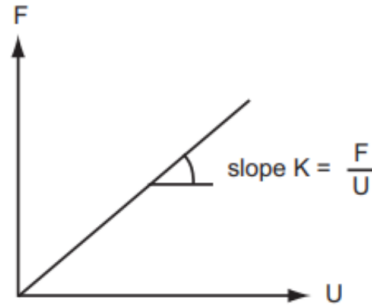


FIGURE 4.1: Load-displacement relationship for an elastic spring structure.

A time independent problem in finite element analysis usually consists of a system of simultaneous equations. This system can be expressed in matrix notation by the following stiffness equation.

$$\{R\} = [K]\{U\}, \quad (4.3)$$

where  $\{R\}$  is the load vector,  $\{U\}$  is the displacement vector and  $[K]$  is the stiffness matrix. If the geometric and material properties of the structure remain constant, the problem is linear. If these properties are dependent either on  $R$  or  $U$ , the problem is nonlinear.

The stiffness matrix of the structure must be established before the load-displacement relationship of the structure can be determined, because once  $K$  is determined, the solution  $U$  follows instantly. Each member or element's load-displacement relationship can alternatively be described in terms of an element stiffness matrix  $k^e$ . With this in mind, the structural stiffness matrix  $K$  is constructed by a systematic superposition of the element stiffness matrices, taking into account the specific arrangement and connection of the elements in the structure.

$$K = \sum_e k^e, \quad (4.4)$$

A continuous structure is represented in Finite Element Analysis by a finite number of discrete elements that connect at their nodes, as stated at the beginning of this chapter. Interpolation functions such as polynomials are used to interpolate the variables inside the element in order to establish geometric compatibility inside and between them. The displacement for element  $m$  is represented by the equation below, which expresses the displacements within an element as a function of the displacements at the  $N$  finite element nodal points:

$$u^{(m)}(x, y, z) = H^{(m)}(x, y, z)\hat{U}, \quad (4.5)$$

where  $H^{(m)}$  is the displacement interpolation matrix,  $m$  is the element number, and  $U$  is a vector containing the three global displacement components  $U_i$ ,  $V_i$ , and  $W_i$  at all nodal points, including those at the element assemblage's supports.

The corresponding element strains can be evaluated as follows:

$$\varepsilon^{(m)}(x, y, z) = B^{(m)}(x, y, z)\hat{U}, \quad (4.6)$$

The rows of  $B^{(m)}$ , where  $B^{(m)}$  is the strain-displacement matrix, are obtained by appropriately differentiating and combining the rows of the matrix  $H^{(m)}$ .

The stresses  $\sigma^{(m)}$  in a finite element are related to the element strains using:

$$\sigma^{(m)} = E^{(m)}(x, y, z)\varepsilon^{(m)}, \quad (4.7)$$

where  $E^{(m)}$  is the elasticity matrix of element  $m$ . The material law specified in  $E^{(m)}$  for each element can be that for an isotropic or an anisotropic material, and can vary from element to element.

In order to relate the nodal forces to the nodal displacements, the element is given a virtual nodal displacement  $\delta^*$  and the external work involving the actual nodal forces  $f$  is equal to the internal work which is formulated by the multiplication of the virtual strain  $\varepsilon^*$  and the actual stress, which is a function of  $\delta^*$  and  $\delta$  respectively. Eq. 4.8 describes the equality between internal and external work.

$$\delta^* f = \int_{vol} [\varepsilon(x, y)^T] \sigma(x, y) dvol, \quad (4.8)$$

Substituting  $\varepsilon^*(x, y)$  from Eq. 4.6 and  $\sigma(x, y)$  from Eq. 4.7 respectively leads to Eq. 4.9

$$f = \left[ \int_{vol} B^T E B dvol \right] \hat{U}, \quad (4.9)$$

The quantity in the square brackets is the element stiffness matrix  $K$ .

## 4.1 Nonlinear Finite Element Analysis

The contrast between the linear and nonlinear reactions of a structure subjected to an external force  $F$  is depicted in Figure 4.2. The stiffness matrix is a function of the structure's geometry and material parameters. If these qualities remain constant, the problem is linear; however, if they change when  $F$  or  $U$  changes, the problem is nonlinear. Both geometric and material nonlinearities are included in the research of the ultimate strength of stiffened panels. As a result, the fundamental aspects of nonlinear structural mechanics solution methodologies are described.

### 4.1.1 Material Nonlinearity

Structural steel is a ductile metallic alloy of Fe and C used extensively in the ship and offshore industries due to its low cost and high modulus of elasticity, which helps maintain small deflections. The mechanical properties of structural materials

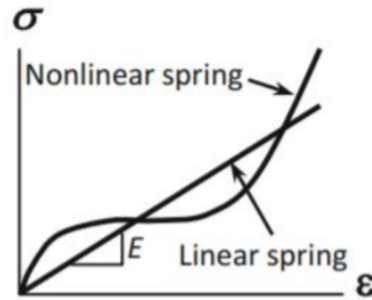


FIGURE 4.2: Linear and nonlinear structural response.

are characterized by testing predesigned specimens under tensile loading. Figure 4.3 shows a schematic of the stress-strain curve for structural steel.

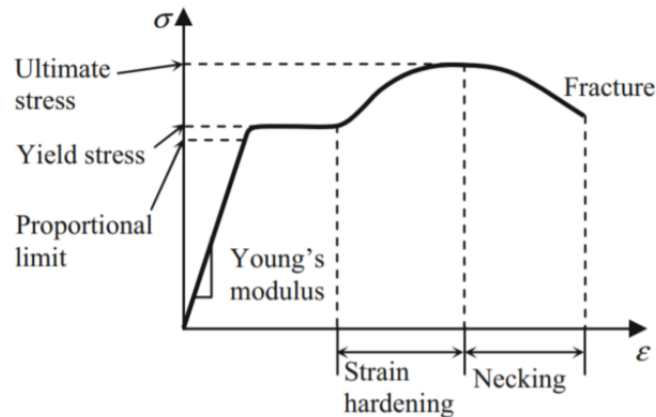


FIGURE 4.3: Typical stress-strain curve for structural steel.

The stress-strain curve is linear in the first part, the stress and strain are proportionate, and the material follows Hooke's Law. The modulus of elasticity ( $E$ ), which is 207 GPa for structural steel, is equal to the slope of this section. The proportionate limit refers to the highest stress at which the stress-strain relationship remains linear. Between the proportional limit and the yield stress is the elastic limit, which is defined as the point at which the most stress can be applied without causing any permanent strain upon unloading. Greater loading causes yield stress, which is the stress that causes 2% strain in structural steel. The strain hardening area begins once the strain has passed the yield point. Additional force is necessary in this region to bend the material to its maximum strength point, which is the highest stress the material can withstand and is known as the ultimate tensile stress. In the early stages of strain hardening, ductile steels usually have a flat region where the strain grows without increasing the stress. The necking region is the third stage, in which a neck forms at the cross sectional area, which becomes much smaller than the original, and finishes with a fracture.

In order to tackle difficult problems, it is usual to make assumptions about the mechanical properties of materials. The most frequent material models are explored after that.

### 4.1.2 Linear Elastic Material Model

This material's response can be divided into two stages. In the first stage, stress is a linear function of strain, with the modulus of elasticity as the proportionality constant ( $E$ ). The second stage begins beyond yield stress and is characterized by a horizontal line with continual produced stress.

If the applied stress is low, the response is linear in the elastic regime and it obeys Hooke's Law, as seen in the first portion of Figure 4.3 and Figure 4.4.

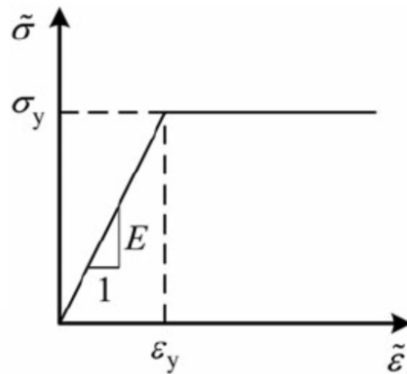


FIGURE 4.4: Elastic-perfectly plastic material.

### 4.1.3 Bilinear Material Model

Because of strain hardening, structural steel may withstand loads beyond the yield stress, as demonstrated in Figure 4.3. This material model is made up of two linear stages. The elastic regime is represented by the first stage, which is a line with slope  $E$ . The second step is an approximation of the real response of the structural steel. Beyond yield stress, the plastic regime is defined by a line of slope  $E_p$ , which is defined as strain hardening tangent modulus with a magnitude of 0.005 to 0.5 times the modulus of elasticity ( $E$ ) (see Figure 4.5). This material model was chosen for the current study because it appeared to be the most suited.

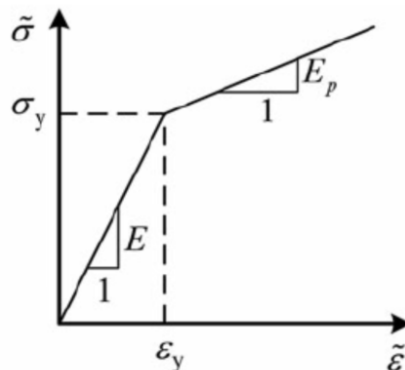


FIGURE 4.5: Bilinear material.

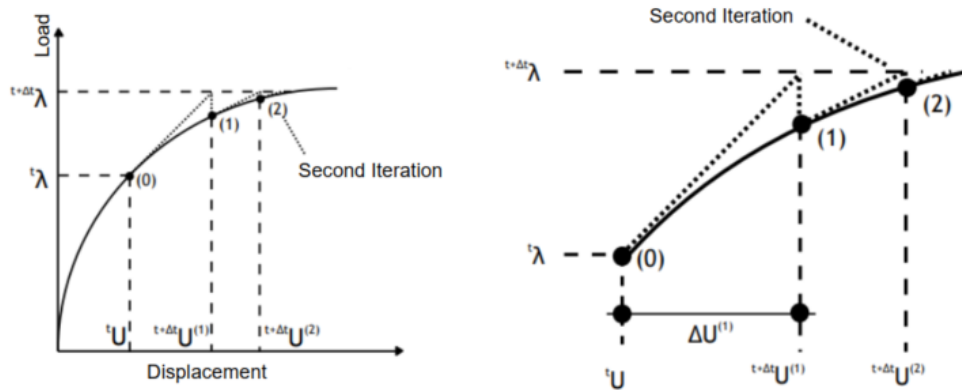


FIGURE 4.6: Schematic of the Newton-Raphson method.

#### 4.1.4 Nonlinear Solution

The most prevalent method for finding the roots of nonlinear equations in finite element studies is Newton-Raphson, which is depicted in Figure 4.6. This method uses a number of iterative techniques to reduce imbalanced forces between external and internal forces while updating the tangent stiffness matrix after each incremental load step. The external load is applied sequentially in nonlinear finite element analysis such that the structure's response is linear. The purpose is to determine the solution at time  $t + \Delta t$ , where  $\Delta t$  is the time increment that corresponds to the required load increase, and the solution  $\bar{u}$  at time  $t$  is presumed to be known. Eq. 4.10 must be satisfied for the structure to be in equilibrium.

$$f(u) = {}^{t+\Delta t} R(u) - {}^{t+\Delta t} F(u), \quad (4.10)$$

where  $u$  is the unknown displacement vector,  $R$  is a known vector composed of the external nodal forces, and  $F(u)$  is the internal forces vector which is a nonlinear function of  $u$ .

In general this solution will not satisfy the system of linear equations exactly and some unbalanced forces are going to exist. If the unbalanced force is lower than a predefined threshold then the iterative procedure has converged else, the procedure repeats.

## 4.2 Finite Element Modeling

### 4.2.1 Material Model

In most modern ships, structural steel is used in the strength deck plating, such as ASTM A131 steel, grade A. In that way, a linear isotropic elastic-plastic material with strain hardening was employed for the finite element simulations with mechanical properties of  $\sigma_y = 235$  MPa,  $E = 210000$  MPa,  $\nu = 0.3$  and  $E_T = 1000$  MPa.

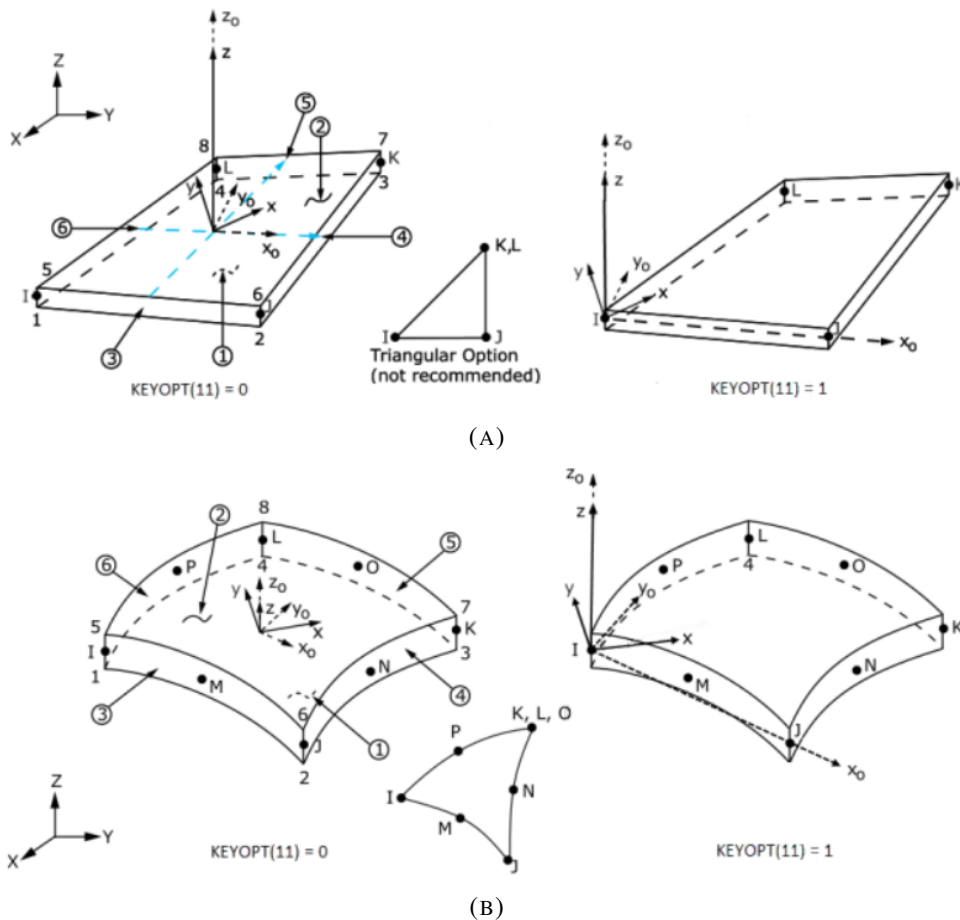


FIGURE 4.7: Geometry demonstrations of a 4-node (A) and a 8-node (B) element.

### 4.2.2 Element Type & Size

A variety of element types are available in FEA commercial software. For the non-linear FEA of thin-walled or plated structures, such as ships, shell elements are preferred. Most software offers two types of shell elements, 4-node and 8-node. The 4-node element has four nodes with three translational and three rotational degrees of freedom at each node, while linear interpolation is used within the element. The 4-node element is well-suited for large rotation and large strain applications. On the other hand, the 8-node element is a quadratic element with eight nodes and six degrees of freedom at each node, three translational and three rotational. 8-node elements are also well-suited for nonlinear applications, and the extra four nodes located at the middle of the sides are capable of capturing the change in geometry's curvature. A visualization of the above considered element types can be shown in Figure 4.7.

A convergence study has been carried out to determine the best element type and size, for a compromise between computational time and accuracy. Multiple simulations have been performed with a variety of element mesh sizes in order to search for the optimal element size that provides a sufficient level of accuracy. In the convergence study of the present mesh, the normalized ultimate stress is monitored for the varying element sizes and element types.

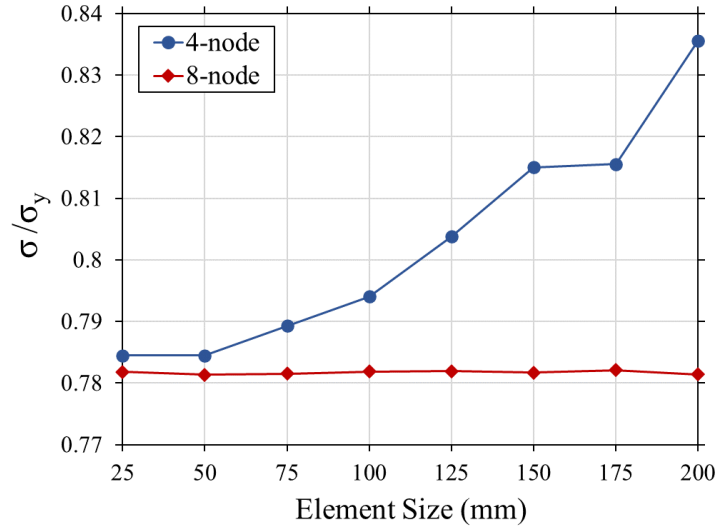


FIGURE 4.8: Mesh convergence study.

Taking into account all the above, 8-node elements were picked since the solution seemed to converge more easily compared to 4-node elements. Finally, an element size of  $(50 \times 50)$  mm was chosen since it provided the most accurate results while taking into account the computational effort needed in order to achieve similar results. Figure 4.8 illustrates the obtained results from the mesh convergence study.

### 4.2.3 Geometrical Initial Imperfections

As with all steel structures, plate panels contain geometric deviations and residual stresses from manufacture and subsequent welding into plate assemblies and, therefore, are not perfectly fair. Due to the complexity and uncertainty of the shape and magnitude of initial imperfections, the latter are usually introduced in the simulations in the form of analytical functions and, more specifically, as Fourier components (DNV, 2021). In this direction, the employed initial local plate imperfection is expressed in the local coordinate system as follows:

$$w(x, y) = w_o \sin\left(\frac{m\pi x}{a}\right) \sin\left(\frac{\pi|y|}{b}\right), \quad (4.11)$$

where  $m$  is the number of half waves as defined in Eq. 2.8.

### 4.2.4 Boundary & Loading Conditions

One key aspect of the FE modeling procedure is the correct application of boundary and loading conditions in order to achieve satisfactory results that not only describe the plate's behavior but also eliminate convergence difficulties associated with the structure's instabilities.

A local coordinate system must first be defined for the right artificial boundary conditions to be applied. Let  $u[x, y, z]$  represent the translational degrees of freedom and  $\theta[x, y, z]$  represent the rotational degrees of freedom, centered on the  $x, y, z$ -coordinates. Also, let "0" on  $u[x, y, z]$  or  $\theta[x, y, z]$  indicate restraint and "1" indicate



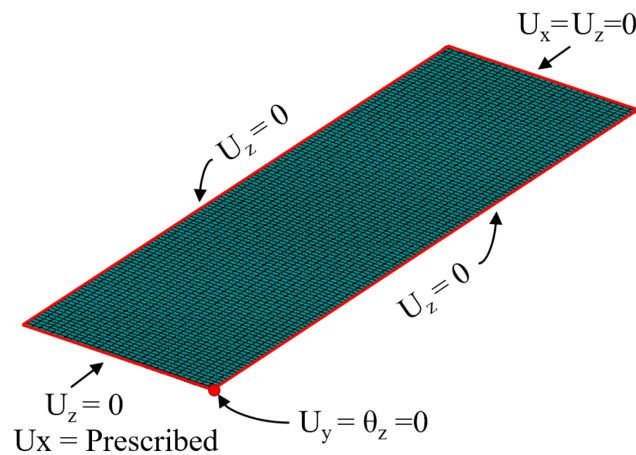


FIGURE 4.9: Plate's boundary and loading conditions.

no restraint. Due to the fact that the target plate is encompassed by longitudinal stiffeners and transverse frames, the edges of the target structure were constrained in the vertical direction  $u[1, 1, 0]$ . Furthermore, at one of the plate's corners, constraints of transverse displacement  $u[1, 0, 0]$  along with rotation around the vertical  $z$ -axis  $\theta[1, 1, 0]$  were applied in order to ensure structural integrity. Lastly, along the target plate's breadth, at one end, an additional constraint was applied in the longitudinal direction  $u[0, 1, 0]$ , while at the loaded end, an appropriate displacement was applied across the longitudinal direction. The imposed boundary and loading conditions of the target structure are shown in Figure 4.9.

It is worth noting that loading conditions were modeled as applied displacement on the plate's cross section instead of force due to the fact that with force control procedure it is difficult to go past the ultimate strength region since the structure has already reached equilibrium and the load starts reducing due to plasticity. By applying an incremental displacement control procedure, such issues can be overcome by gradually increasing the applied displacement and measuring the corresponding reaction force. Also, the aforementioned method is chosen since it is more suitable for overcoming convergence difficulties associated with buckling instabilities.

#### 4.2.5 FE Model Validation

According to the evaluated results (see Figure 4.10a) and the load-displacement behavior of a plate subjected to compressive stresses, a load level less than the bifurcation point  $D$  corresponds to a state with a fully elastic response and a small out of plane deflection (points  $A$ ,  $B$ , and  $C$ ). Point  $D$  marks the initiation of plasticity where the plate buckles, forming  $m$  number of half-waves across its length. At this point, the fibers in the direction of compression have shortened while the fibers perpendicular to the stress direction lengthen. Plastic strain is propagated further at point  $E$  until a critical load level is reached at point  $F$ , resulting in a state of ultimate plastic yield at ultimate strength. The above observed results validate the elastic buckling theory of simply supported plates subjected to uniform compression.

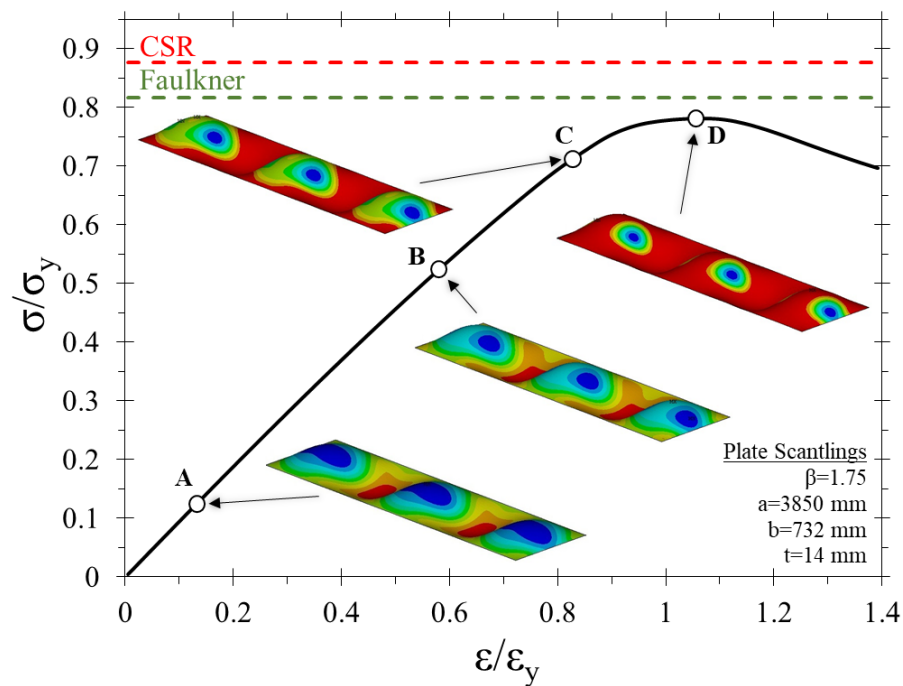
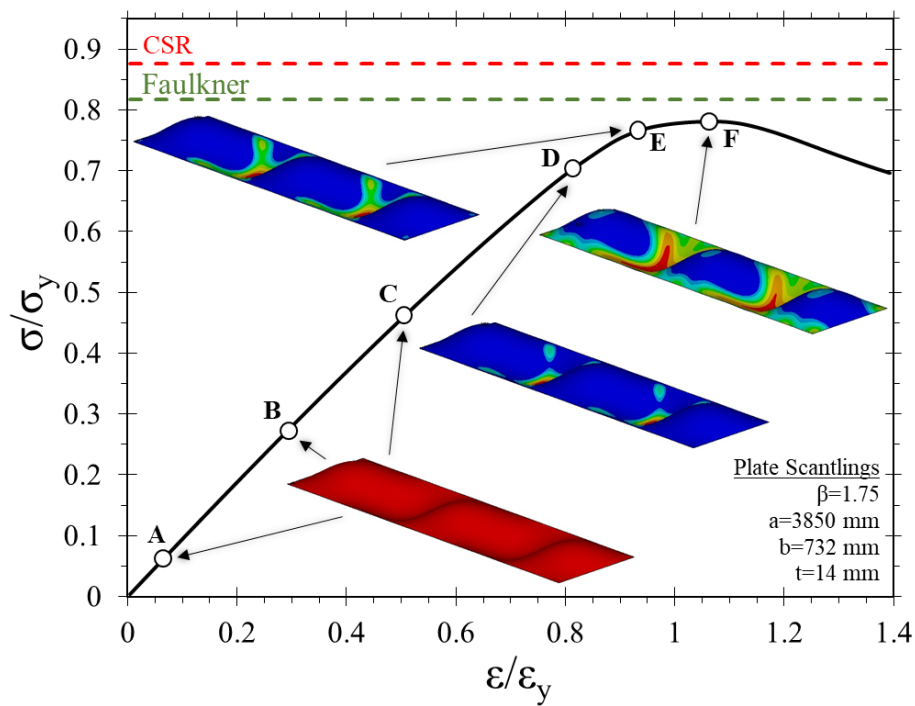


FIGURE 4.10: Phases of plastic strain (A) and von Mises stress (B).

Notes: In the contour plots, the plate's plastic strain and von Mises stress state is visualized at each respective point. The colors are mapped over the geometry to indicate the result values at each location in the model. High color contrast indicates areas of greater plastic strain intensity.

## Chapter 5

# Probabilistic Modeling

### 5.1 Monte Carlo Simulation

In the scope of the proposed work, a Monte Carlo Simulation was used. In general, simulation is a technique for conducting experiments in a laboratory or on a computer to model the behavior of a system. Usually, simulation models result in "simulated" data that must be treated statistically to predict the future behavior of the system. In this broad sense, simulation has been used as a predictive tool for economic systems, business environments, war games, and management games.

The name "Monte Carlo method" was introduced in 1944 by von Neumann and Ulam as a code name for their secret work on neutron diffusion problems at the Los Alamos Laboratory. The name was chosen apparently because of the association of the town of Monte Carlo with roulette, which is one of the simplest tools that can be used for generating random numbers.

A Monte Carlo simulation is usually used for problems involving random variables with known or assumed probability distributions. Using statistical sampling techniques, a set of values for the random variables are generated in accordance with the corresponding probability distributions. These values are treated similarly to a sample of experimental observations and are used to obtain a "sample" solution. By repeating the process and generating several sets of sample data, many sample solutions can be determined. Statistical analysis of the sample solutions is then performed.

The Monte Carlo method thus consists of three basic steps:

- a) Simulation of the random variables and generation of several sample data sets using statistical sampling techniques.
- b) Solutions using the sampled data.
- c) Statistical analysis of the results.

Because the results from the Monte Carlo technique depend on the number of samples used, they are not exact and subject to sampling errors. Generally, the accuracy increases as the sample size increases.

Sampling from a particular probability distribution involves the use of random numbers. Random numbers are essentially random variables uniformly distributed over the unit interval  $[0,1]$ . Many codes are available for computers to generate a sequence of "pseudo" random digits where each digit occurs with approximately equal probability. The generation of such random numbers plays a central role in

the generation of a set of values (or realizations) of a random variable that has a probability distribution other than the uniform probability law. The Monte Carlo method is considered one of the most powerful techniques for analyzing complex problems due to the enormous computing power of computers.

## 5.2 Surrogate Modeling

MCSs require a high order of magnitude number of statistical experiments, which in our case are to be based on numerical FE simulations. This poses the problem that these are time-consuming for the scope of this approach. In order to significantly narrow down the number of required FE simulations for the sake of time efficiency without sacrificing accuracy, meta-modeling based on surrogates was employed. The main concept is to perform FE simulations on key sample points within the design space and then fit an analytical formula, which later may be used as a surrogate model for MCS.

### 5.2.1 Design of Experiments

Design of experiments (DOE) is a branch of applied statistics that deals with planning, conducting, analyzing, and interpreting controlled tests to evaluate the factors that control the value of a parameter or group of parameters. Usually, DOE is used to map a response surface over a particular region of interest in order to optimize the output of the process or to select the operation points to achieve a specific outcome. In reviewing the literature that uses DOE in numerical experimentation, various types of DOE, such as RSM (Anyfantis, 2020), central composite design (CCD) (Anyfantis, 2020), one factor at a time (Anyfantis, 2019), full factorial (Anyfantis, 2019), Taguchi methodology (Kim, 2010) and low cost response surface methodology (Koç et al., 2000), have been deployed.

### 5.2.2 Response Surface Methodology

The response surface methodology (RSM) consists of mathematical and statistical techniques and is used extensively for the optimization of processes influenced by many interrelated factors. The goal of the RSM is to create an approximating model for a system's response ( $y$ ), when the actual relationship between its controllable input variables ( $X_1, X_2, X_3, \dots, X_N$ ) and its response variable ( $y$ ) is unknown, e.g.,  $y = f(X_1, X_2, X_3, \dots, X_N)$ , where  $f$  is an unknown function regarded as a meta-model. The approximating empirical model is based on observed data from the system and is usually a low-order polynomial  $y = g(X_1, X_2, X_3, \dots, X_N)$ , where,  $g$  is the approximating function.

Among the wide family of surrogates, the faced central composite design (see Figure 5.1) was employed for generating the key sample points due to the simplicity of the response within the design space (Anyfantis, 2019). Since we have three RVs and according to this particular sampling setting, a total of 15 samples ( $2^3$  full factorial +  $2 \cdot 3$  face centered + 1 center of mass) per slenderness ratio are to be simulated in FEA. The three-dimensional cube structure models yield the sampling points of

three different factors, i.e.,  $X_1$ ,  $X_2$  and  $X_3$ , which in turn correspond to representations of the RV related to the yield stress, Young's modulus, and bow imperfection, respectively.

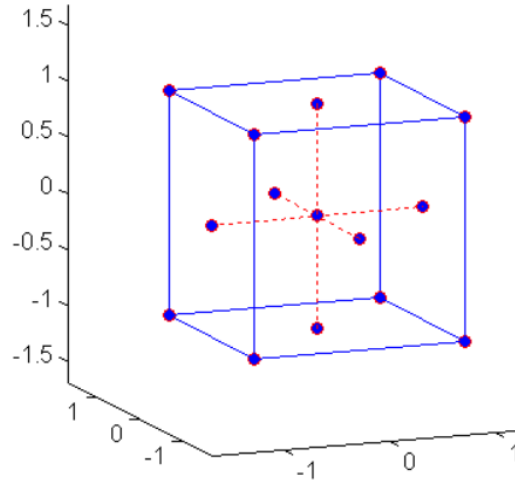


FIGURE 5.1: Illustration of faced central composite design sampling for surrogate modeling. (Figure borrowed from Matlab documentation.)

The lower limit of each factor (-1) is equivalent to the representation of the 5% lower bound, the central point (0) is equivalent to the median, and the higher limit (1) to the 95% upper bound of each RV. By considering the statistical structures of each RV, the parameters used for the FE simulations performed per slenderness ratio are listed in Table 5.1.

TABLE 5.1: Experiment matrix for surrogate modeling generation through FE simulations.

Sample	$X_1$	$w_o$ [mm]	$X_2$	$\sigma_y$ [MPa]	$X_3$	$E$ [GPa]
1	-1	1.46	-1	250.38	-1	189
2	-1	1.46	-1	250.38	1	231
3	-1	1.46	1	321.50	-1	189
4	-1	1.46	1	321.50	1	231
5	1	5.03	-1	250.38	-1	189
6	1	5.03	-1	250.38	1	231
7	1	5.03	1	321.50	-1	189
8	1	5.03	1	321.50	1	231
9	-1	1.46	0	283.72	0	210
10	1	5.03	0	283.72	0	210
11	0	2.71	-1	250.38	0	210
12	0	2.71	1	321.50	0	210
13	0	2.71	0	283.72	-1	189
14	0	2.71	0	283.72	1	231
15	0	2.71	0	283.72	0	210



## Chapter 6

# Results - Discussion

### 6.1 RSM Results

As discussed in section 5.2.2, the second-order model with quadratic parameters is widely used. The general form of the multi-factor response is given by:

$$\bar{Y} = \beta_o + \sum_{i=1}^k c_i x_i + \sum_{i=1}^k c_{ii} x_i^2 + \sum_{i=1 \leq i < j \leq k} c_{ij} x_i x_j + \varepsilon, \quad (6.1)$$

where,  $c_{ii}$  represents the coefficients of the quadratic factors.

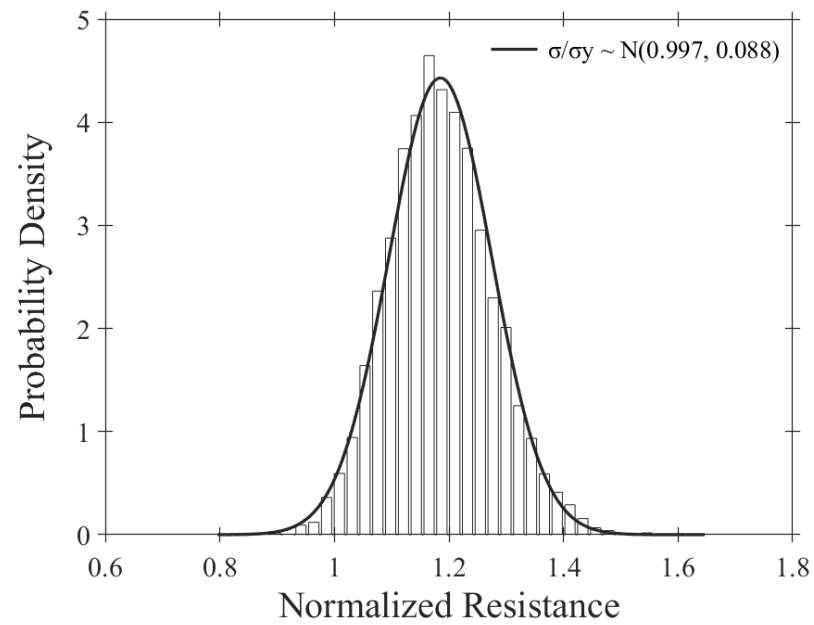
In our particular case, where three RVs are involved, the preceding equation may be written as follows:

$$\begin{aligned} \sigma_{ult} = & c_o + c_1 \sigma_y + c_2 E + c_3 w_o + c_{12} \sigma_y E + \\ & + c_{13} \sigma_y w_o + c_{23} w_o E + c_{11} \sigma_y^2 + c_{22} E^2 + c_{33} w_o^2, \end{aligned} \quad (6.2)$$

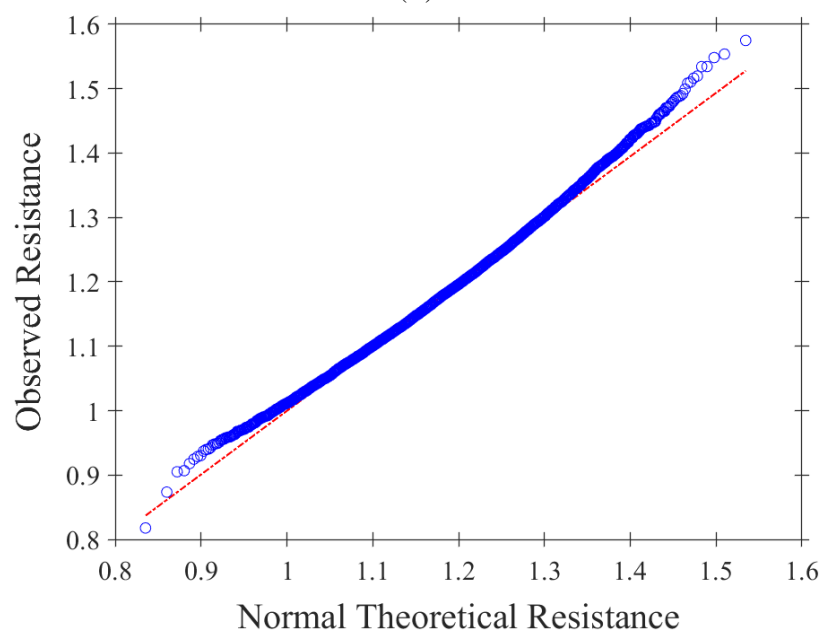
The ten coefficients of the polynomial are obtained through a least-square fit over the fifteen numerically obtained resistances as per the CCD sampling scheme. The accuracy of the regression function can be estimated from the correlation coefficient of determination  $R^2$ , which represents the relevant difference between the design point and the result according to the proposed formula. In all cases, very high accuracy has been reached. Table 6.1 lists the corresponding coefficients of the polynomial that represent the surrogate model along with their respective correlation coefficients for all three slenderness ratio cases.

### 6.2 MCS Results

A Monte Carlo Simulation (MCS) for each slenderness ratio level has been performed through the random independent generation of 10,000 samples based on the parametric statistical models of each defined RV. The sampling was supported by the Latin Hypercube stratified method. For illustration purposes, Figure 6.2 presents joint pair distributions of the input RVs. Furthermore, a histogram of a plate's normalized resistance has been generated and presented in Figure 6.1a along with a Q-Q plot in Figure 6.1b in order to assess its statistical structure. As it is illustrated, the data follows a linear trend, which indicates that a Gaussian parametric model is considered as the statistical structure representing the entire population for the probabilistic representation of the resistance.



(A)



(B)

FIGURE 6.1: Statistical analysis of normalized resistance with the aid of a histogram (A) and a Q-Q plot (B).



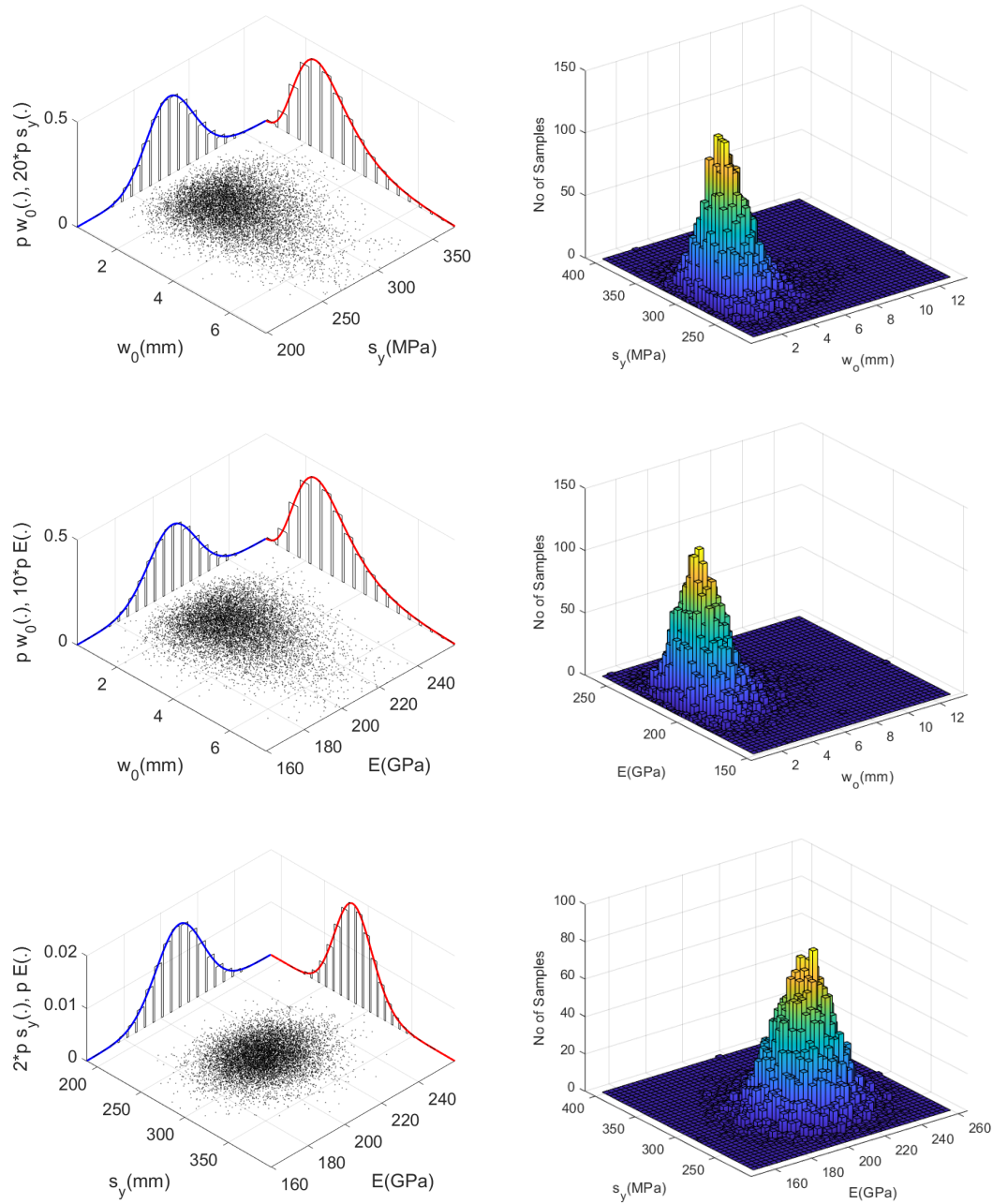


FIGURE 6.2: Latin Hypercube sampling for MCS visualized through pairs of RVs.

TABLE 6.1: Coefficients of the RS obtained from the finite elements simulation.

RS coeff.	$\beta=1$	$\beta=1.75$	$\beta=2.5$
$c_0$	23.0015	7.7567	0.9098
$c_1$	0.7343	0.4475	0.3376
$c_2$	1.71e-4	5.37e-4	3.54e-4
$c_3$	-0.2958	-6.0936	-0.5056
$c_{12}$	5.40e-7	1.60e-6	4.54e-7
$c_{13}$	-0.0226	0.0089	0.0075
$c_{23}$	2.22e-5	-4.78e-5	-2.18e-5
$c_{11}$	0.0003	-0.0006	-0.0002
$c_{22}$	-8.46e-10	-1.11e-9	-3.09e-10
$c_{33}$	-0.3045	0.9275	0.0760
$R^2$	0.998	0.999	0.999

### 6.3 Probabilistic Buckling Curves

An aggregation of the reliability analysis results is presented in Figure 6.3, where the unified probability density function (PDF) of the resistance was calculated by averaging the sample statistics obtained from all three considered slenderness ratios. The statistical structure per slenderness ratio follows an intuitive and expected trend, with the resistance's center of mass (population mean) lowering as the slenderness ratio increases due to the increasing effect of the structural instability collapse mode in more slender plates. Also, it must be noted that the variance reduces as well. For illustration purposes, the 0.1% and 0.01% ( $p_f = 10^{-3}$  and  $p_f = 10^{-4}$  respectively) lower confidence bound resistance levels per slenderness ratio and their respective regressions are presented. Such regressions for the probabilistic resistance may serve as an alternative to the empirically based resistance curves derived from the formulations presented in section 2.3

Finally, in Figure 6.4, the probability of failure for each empirical formula is presented, in percentile, with respect to the probabilistic resistance calculated per slenderness ratio. It is observed that for a low slenderness ratio, all empirical formulations are characterized by a conservative design threshold, whereas for medium to high values of plate slenderness ratio, a high probability of failure is associated with von Karman's, Schnadel's and Frankland's formulations compared to Box's and Faulkner's, which follow the trend of a low probability of failure across all plate slenderness ratios.

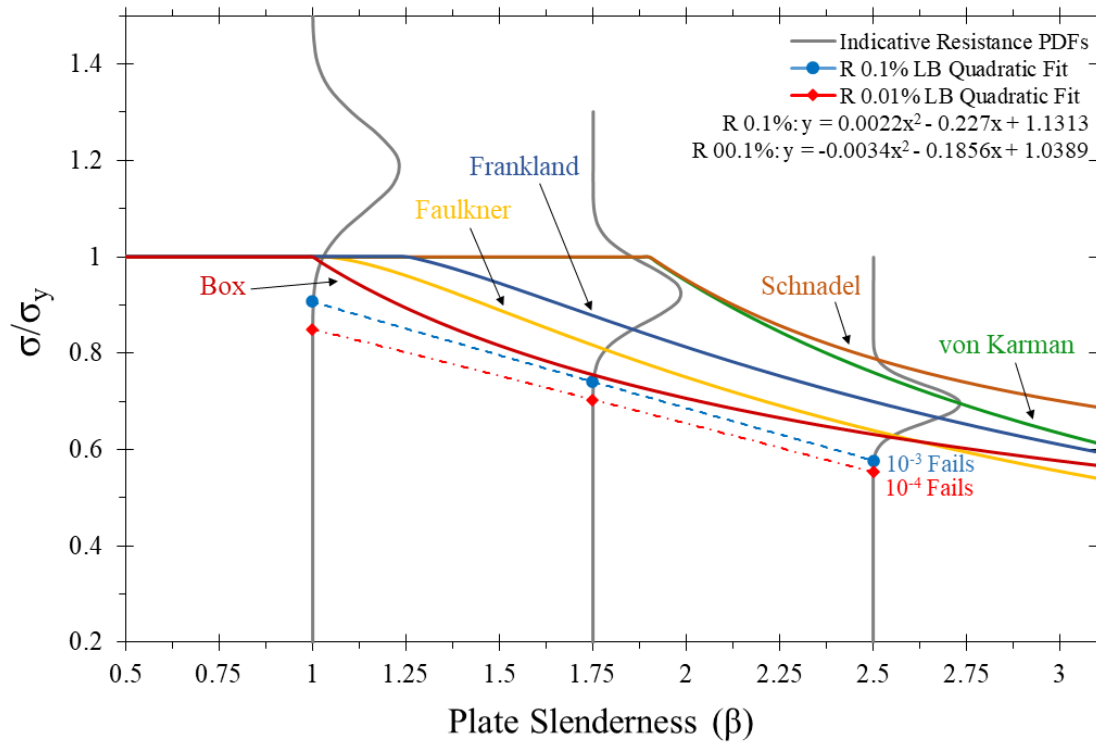


FIGURE 6.3: Probabilistic resistance curves (buckling curves).

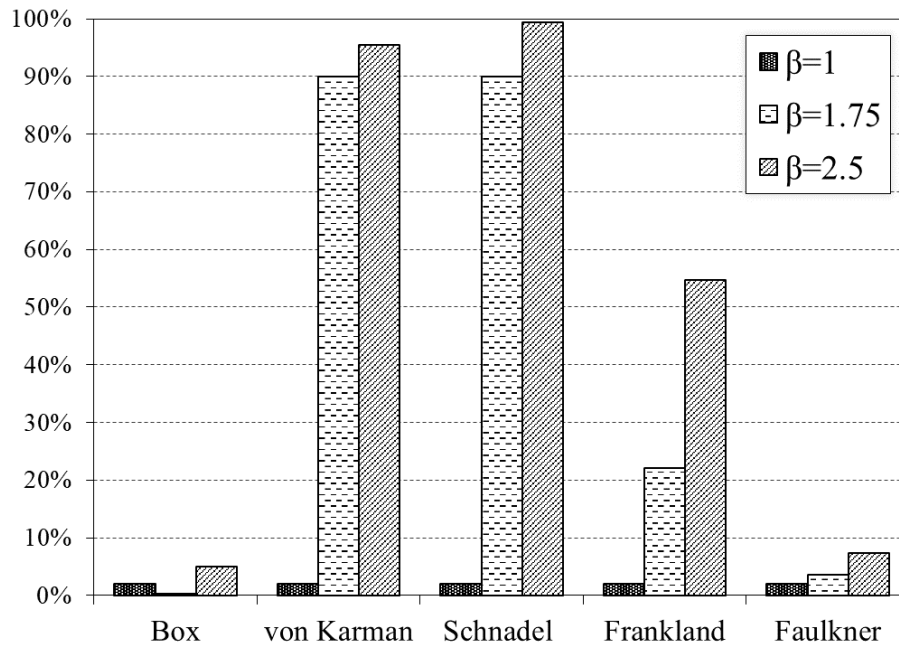


FIGURE 6.4: Probability of failure for each empirical model per slenderness ratio.

## 6.4 Proposed Safety Factors (PSFs)

According to Rahman et al., 2017, PSFs for the ultimate load-carrying capacity of plates can be determined using the reliability indexing method. The following equation shows the relationship between the PSF and the reliability index:

$$\mu - \beta_T \sigma = \frac{1}{\gamma} f_N, \quad (6.3)$$

where  $\mu$  and  $\sigma$  are the mean and the standard deviation of the normalized ultimate buckling strength, respectively,  $\beta_T$  is the target reliability index,  $\gamma$  is the partial safety factor, and  $f_N$  is the corresponding nominal strength. Figure 6.5 illustrates Eq. 6.3 graphically for RR = 0.8.

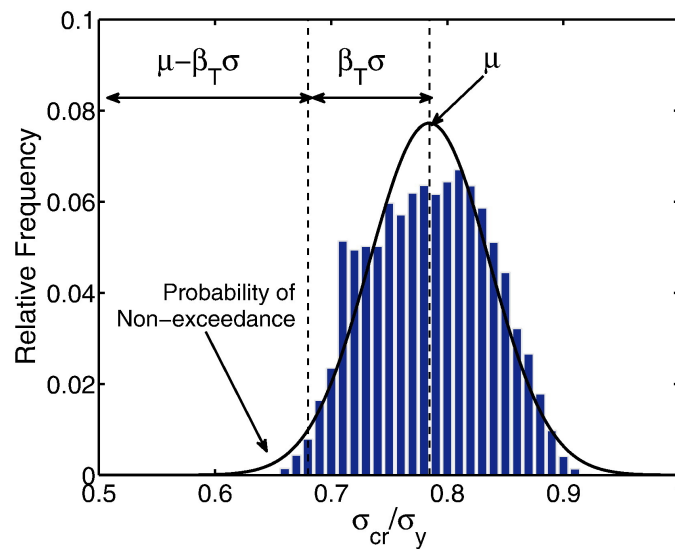


FIGURE 6.5: Explanation of Eq. 6.3 (Rahman et al., 2017).

Assuming that the probability density function for the ultimate buckling strength is normally distributed, the designer can opt for a desired safety factor based on his risk tolerance, considering the obtained statistical structure of the selected slenderness ratio.

## Chapter 7

# Conclusions

This work focuses on the development of probabilistic buckling models that can be used within the design of steel plates used in ship structures and their comparison to the empirical formulae found in rules and in the scientific literature. Findings have shown that the design zone threshold suggested by the empirical buckling resistance curves is associated with a high probability of failure for a medium-to-high value of plate slenderness compared to the probabilistic resistance curves generated by the MCS. Finally, the notion of proposed safety factors is briefly discussed in order to demonstrate the motive of modeling plate buckling in a probabilistic approach. This work is believed to support the transition to a risk-based design where probabilistic treatment of all involved uncertainties is required.



# Bibliography

- Anyfantis, Konstantinos N. (2019). “Evaluating the influence of geometric distortions to the buckling capacity of stiffened panels”. In: *Thin-Walled Structures* 140, pp. 450–465. ISSN: 0263-8231. DOI: <https://doi.org/10.1016/j.tws.2019.03.057>. URL: <https://www.sciencedirect.com/science/article/pii/S0263823118312473>.
- (2020). “Ultimate strength of stiffened panels subjected to non-uniform thrust”. In: *International Journal of Naval Architecture and Ocean Engineering* 12, pp. 325–342. ISSN: 2092-6782. DOI: <https://doi.org/10.1016/j.ijnaoe.2020.03.003>. URL: <https://www.sciencedirect.com/science/article/pii/S2092678220300054>.
- Box, Thomas (1883). *A practical Treatise on the Strength of Materials: Including Their Elasticity and Resistance to Impact*. London, U.K.: E. & F.N. Spon.
- Chryssanthopoulos, Marios K. (1998). “Probabilistic buckling analysis of plates and shells”. In: *Thin-Walled Structures* 30.1, pp. 135–157. ISSN: 0263-8231. DOI: [https://doi.org/10.1016/S0263-8231\(97\)00035-9](https://doi.org/10.1016/S0263-8231(97)00035-9). URL: <https://www.sciencedirect.com/science/article/pii/S0263823197000359>.
- DNV (2021). *DNV-CG-0128 - Edition 2021-09*. Høvik, Norway: Det Norske Veritas group.
- Dou, Chao and Yong-Lin Pi (2016). “Effects of Geometric Imperfections on Flexural Buckling Resistance of Laterally Braced Columns”. In: *Journal of Structural Engineering* 142.9, p. 04016048. DOI: [10.1061/\(ASCE\)ST.1943-541X.0001508](https://doi.org/10.1061/(ASCE)ST.1943-541X.0001508).
- Faulkner, Douglas (Mar. 1975). “A Review of Effective Plating for Use in the Analysis of Stiffened Plating in Bending and Compression”. In: *Journal of Ship Research* 19.01, pp. 1–17. ISSN: 0022-4502. DOI: [10.5957/jsr.1975.19.1.1](https://doi.org/10.5957/jsr.1975.19.1.1). URL: <https://doi.org/10.5957/jsr.1975.19.1.1>.
- Frankland, JM. (1940). *The strength of ship plating under edge compression*. Washington DC, USA: US Experimental Model Basin Progress Report 469.
- Hughes, Owen and Jeom Kee Paik (2010). *Ship Structural Analysis and Design*. 01 Pavonia Avenue Jersey City, New Jersey 07306: The Society of Naval Architects and Marine Engineers.
- IACS (2021a). *Common Structural Rules for Bulk Carriers and Oil Tankers - 01 Jan 2021*. London: International Association of Classification Societies.
- (2021b). *Shipbuilding and Repair Quality Standard - Rec. 47 Rev.10 Sep 2021*. London: International Association of Classification Societies.
- Ivanov, Lyuben D. (2013). “Reliability estimation of ship’s hull girder in probabilistic terms when ultimate strength is used as a failure mode”. In: *Ships and Offshore Structures* 8.2, pp. 141–153. DOI: [10.1080/17445302.2012.664400](https://doi.org/10.1080/17445302.2012.664400). eprint: <https://doi.org/10.1080/17445302.2012.664400>. URL: <https://doi.org/10.1080/17445302.2012.664400>.

- Kala, Zdenek (Oct. 2007). “Stability problems of steel structures in the presence of stochastic and fuzzy uncertainty”. In: *Thin-walled Structures - THIN WALL STRUCT* 45, pp. 861–865. DOI: [10.1016/j.tws.2007.08.007](https://doi.org/10.1016/j.tws.2007.08.007).
- Karman, Theodore von (1924). *Die mittragende Breite (The effective width)*. Berlin: Springer.
- Kim, Hong Seok (2010). “A combined FEA and design of experiments approach for the design and analysis of warm forming of aluminum sheet alloys”. In: *The International Journal of Advanced Manufacturing Technology* 51, pp. 1–14.
- Koç, Muammer et al. (Dec. 2000). “Use of FEA and design of experiments to establish design guidelines for simple hydroformed parts”. In: *International Journal of Machine Tools and Manufacture* 40, pp. 2249–2266. DOI: [10.1016/S0890-6955\(00\)00047-X](https://doi.org/10.1016/S0890-6955(00)00047-X).
- Melcher, Jindřich et al. (2004). “Design characteristics of structural steels based on statistical analysis of metallurgical products”. In: *Journal of Constructional Steel Research* 60.3. Eurosteel 2002 Third European Conference on Steel Structures, pp. 795–808. ISSN: 0143-974X. DOI: [https://doi.org/10.1016/S0143-974X\(03\)00144-5](https://doi.org/10.1016/S0143-974X(03)00144-5). URL: <https://www.sciencedirect.com/science/article/pii/S0143974X03001445>.
- Rahman, Mahmudur et al. (2017). “Probabilistic ultimate buckling strength of stiffened plates, considering thick and high-performance steel”. In: *Journal of Constructional Steel Research* 138, pp. 184–195. ISSN: 0143-974X. DOI: <https://doi.org/10.1016/j.jcsr.2017.07.004>.
- Rahman, Mahmudur et al. (2020). “Probabilistic Compressive Strength of Stiffened Steel Plates Exhibiting Column-Like Behavior: Ultimate and Serviceability Limit States”. In: *Journal of Structural Engineering* 146.9, p. 04020166. DOI: [10.1061/\(ASCE\)ST.1943-541X.0002719](https://doi.org/10.1061/(ASCE)ST.1943-541X.0002719).
- Schnadel, G. (1930). *Die überschreitung der knickgrenze dunnen platen*. Stockholm: Proceedings of the 3rd International Congress on Applied Mechanics.
- Zhang, Shengming (2016). “A review and study on ultimate strength of steel plates and stiffened panels in axial compression”. In: *Ships and Offshore Structures* 11.1, pp. 81–91. DOI: [10.1080/17445302.2014.992610](https://doi.org/10.1080/17445302.2014.992610). eprint: <https://doi.org/10.1080/17445302.2014.992610>. URL: <https://doi.org/10.1080/17445302.2014.992610>.



## Appendix A

# Matlab Source Code

```

1  clc
2  clear
3  close all
4
5  %*****
6  %----- CALCULATIONS SECTION -----
7  %*****
8
9  sNom=235;
10 ENom=210000;
11 v=0.3;
12 Plate_Slenderness=1;
13
14
15 %=====
16 % Random variable distributions
17 %=====
18 % m=Mean, S=Standard deviation
19 msy=5.647885875;
20 Ssy=0.075463613;
21 mE=210;
22 SE=12.6;
23 mw0=0.997;
24 Sw0=0.376;
25
26
27 %=====
28 % Latin hypercube sampling
29 %=====
30 X = lhsdesign(10000,3);
31
32
33 %=====
34 % Generation of samples
35 %=====
36 sy=zeros(10000,1);
37 E=zeros(10000,1);
38 w0=zeros(10000,1);
39
40 for i=1:10000
41     sy(i)=logninv(X(i,2),msy,Ssy);
42     E(i)=norminv(X(i,3),mE,SE);
43     w0(i)=logninv(X(i,1),mw0,Sw0);

```

```

44 end
45 Samples=[sy,E,w0];
46
47
48 %=====
49 % sUlt calculation
50 %=====
51 sUlt=zeros(10000,1);
52 sUlt_Normalized=zeros(10000,1);
53 for i=1:10000
54     sUlt(i)=(1653513388313759*sy(i))/2251799813685248 + ...
        (6148550398687*E(i))/36028797018963968 - ...
        (5328169876444943*w0(i))/18014398509481984 + ...
        (638068171733401*sy(i)*E(i))/1180591620717411303424 - ...
        (6508901971710557*sy(i)*w0(i))/288230376151711744 + ...
        (3281781738237517*E(i)*w0(i))/147573952589676412928 + ...
        (701820137058097*sy(i)^2)/2305843009213693952 - ...
        (4089481968072747*E(i)^2)/4835703278458516698824704 - ...
        (685747744451703*w0(i)^2)/2251799813685248 + ...
        3237167866593989/140737488355328;
55     sUlt_Normalized(i)=sUlt(i)/sNom;
56 end
57
58 sUlt_mean=mean(sUlt);
59 sUlt_stdev=std(sUlt);
60 sUlt_max=max(sUlt);
61 sUlt_min=min(sUlt);
62
63 %Normal pdf for sUlt
64 pd_sUlt=fitdist(sUlt,'Normal');
65 confidence_95=paramci(pd_sUlt);
66
67 %Normal pdf for Normalized sUlt
68 pd_sUlt_Normalized=fitdist(sUlt_Normalized,'Normal');
69
70 %Maximum resistance of 0.1% of the weakest columns
71 sUlt_01=icdf(pd_sUlt_Normalized,0.001);
72
73 %Maximum resistance of 0.01% of the weakest columns
74 sUlt_001=icdf(pd_sUlt_Normalized,0.0001);
75
76
77 %=====
78 % Empirical Models Calculation
79 %=====
80
81 %Box critical stress calculation:
82 s_Box=sNom/(Plate_Slenderness^0.5);
83 if s_Box>sNom
84     s_Box=sNom;
85 end
86 p_failure_Box=cdf(pd_sUlt_Normalized,s_Box/sNom);
87
88
89 %von Karman critical stress calculation:
90 s_von_Karman=(1.9*sNom)/Plate_Slenderness;
91 if s_von_Karman>sNom

```

```

92     s_von_Karman=sNom;
93 end
94 p_failure_von_Karman=cdf(pd_sUlt_Normalized,s_von_Karman/sNom);
95
96
97 %Schnadel critical stress calculation:
98 s_Schnadel=0.5*sNom+(1.81*sNom)/Plate_Slenderness^2;
99 if s_Schnadel>sNom
100     s_Schnadel=sNom;
101 end
102 p_failure_Schnadel=cdf(pd_sUlt_Normalized,s_Schnadel/sNom);
103
104
105 %Frankland critical stress calculation:
106 s_Frankland=(2.25*sNom)/Plate_Slenderness-(1.25*sNom)/
107 Plate_Slenderness^2;
108 if s_Frankland>sNom
109     s_Frankland=sNom;
110 end
111 p_failure_Frankland=cdf(pd_sUlt_Normalized,s_Frankland/sNom);
112
113
114 %Faulkner critical stress calculation:
115 s_Faulkner=(2*sNom)/Plate_Slenderness-sNom/Plate_Slenderness^2;
116 if s_Faulkner>sNom
117     s_Faulkner=sNom;
118 end
119 p_failure_Faulkner=cdf(pd_sUlt_Normalized,s_Faulkner/sNom);
120
121
122 %=====
123 % Saving statistical parameters into a .txt file
124 %=====
125 %save ('Parameters.txt', 'Samples', '-ascii')
126
127
128
129
130 %*****
131 %----- CHARTS SECTION -----
132 %*****
133
134 %=====
135 % Normalized sUlt probability distribution + Bins
136 %=====
137 figure
138 hold on
139
140 %Define limits of plotting
141 XNom = (min(sUlt)-1*std(sUlt):0.1:max(sUlt)+1*std(sUlt))/sNom;
142
143 %Define critical stress distribution
144 Normalized_sUlt_pdf = ...
145     normpdf(XNom,mean(sUlt/sNom),std(sUlt/sNom));
146
147 %Plot histogram with distribution
148 [n_x, xout] = hist(sUlt/sNom,30); %creates 30 bins

```

```

148 n_x = n_x ./ ( sum(n_x) *(xout(2)-xout(1))); %normalize to ...
      be a pdf
149 [r,r,r,x_Pos,x_Height] = makebars(xout,n_x);
150 plot(XNom, ...
      Normalized_sUlt_pdf, '-k', 'DisplayName', 'Probability ...
      Density', 'LineWidth', 2); %pdf
151 plot(x_Pos, x_Height, '-k') %histogram
152
153
154 xlabel('Normalized Resistance');
155 ylabel('Probability Density');
156 box on;
157 set(gca, 'TickDir', 'both');
158 set(gca, 'fontname', 'Times New Roman');
159 set(gca, 'TickDir', 'both');
160 legend
161
162
163 %=====
164 % Q-Q Plot
165 %=====
166 figure
167
168 qqplot(sUlt_Normalized,pd_sUlt_Normalized)
169 box on;
170 set(gca, 'TickDir', 'both');
171 set(gca, 'fontname', 'Times New Roman')
172 % set(gca, 'XMinorTick', 'on', 'YMinorTick', 'on')
173
174
175 %=====
176 % Sampling Scatters with distributions
177 %=====
178
179 %-----w0, sy scatter with ...
      distributions-----
180 %Define limits of plotting
181 X = min(w0):0.1:max(w0)-5;
182 Y = mean(sy)-4*std(sy):1:mean(sy)+4*std(sy);
183
184 %2-d Mean and St.dev. matrix
185 MeanVec = [mean(w0) mean(sy)];
186 StdVec= [std(w0), std(sy)];
187
188 %Get the 1-d PDFs for the "walls"
189 Z_x = ...
      lognpdf(X, log(MeanVec(1)^2/sqrt(MeanVec(1)^2+StdVec(1)^2)),
190 sqrt(log(1+(StdVec(1)/MeanVec(1))^2)));
191 Z_y = ...
      lognpdf(Y, log(MeanVec(2)^2/sqrt(MeanVec(2)^2+StdVec(2)^2)),
192 sqrt(log(1+(StdVec(2)/MeanVec(2))^2)));
193
194 %Scale the y-axis pdf to be equal (modify xlabel below ...
      accordingly)
195 Scale_y=20;
196
197 %Get the 2-d samples for the "floor"

```

```

198 Samples = [w0, sy];
199
200 figure; hold on;
201 %Plot the samples on the "floor"
202 plot3(Samples(:,1),Samples(:,2),zeros(size(Samples,1),1),'k.',
203 'MarkerSize',2)
204
205 %Plot the histograms on the walls from the data in the middle
206 [n_x, xout] = hist(Samples(:,1),30); %creates 30 bars, ...
    n_x=number of elements in each beam, xout=bin limits
207 n_x = n_x ./ ( sum(n_x) * (xout(2)-xout(1)));%Normalizes to ...
    be a pdf
208 [x_Pos, x_Height] = makebars(xout,n_x);%Creates the bar ...
    points
209 plot3(x_Pos, Y(end)*ones(size(x_Pos)),x_Height, '-k')
210
211 %Now plot the other histograms on the wall
212 [n_y, yout] = hist(Samples(:,2),20);
213 n_y = n_y ./ ( sum(n_y) * (yout(2)-yout(1)));
214 [y_Pos, y_Height] = makebars(yout,n_y);
215 plot3(X(1)*ones(size(y_Pos)),y_Pos, Scale_y*y_Height, '-k')
216
217 %Now plot the 1-d pdfs over the histograms
218 plot3(X, ones(size(X))*Y(end), Z_x, '-r', 'LineWidth',2);
219 plot3(ones(size(Y))*X(1), Y, Scale_y*Z_y, '-b', 'LineWidth',2);
220
221 %Make the figure look nice
222 grid on; view(45,55);
223 xlabel('w_0 (mm)'), ylabel('s_y (MPa)'), zlabel('p w_0(.), 20*p ...
    s_y(.)')
224 axis([X(1) X(end) Y(1) Y(end)])
225 title('Latin hypercube sampling')
226
227 %-----w0, E scatter with ...
    distributions-----
228 %Define limits of plotting
229 X = min(w0):0.1:max(w0)-5;
230 Y = mean(E)-4*std(E):1:mean(E)+4*std(E);
231
232 %2-d Mean and St.dev. matrix
233 MeanVec = [mean(w0) mean(E)];
234 StdVec= [std(w0),std(E)];
235
236 %Get the 1-d PDFs for the "walls"
237 Z_x = ...
    lognpdf(X,log(MeanVec(1)^2/sqrt(MeanVec(1)^2+StdVec(1)^2)),
238 sqrt(log(1+(StdVec(1)/MeanVec(1))^2)));
239 Z_y = normpdf(Y,MeanVec(2),StdVec(2));
240
241 %Scale the y-axis pdf to be equal (modify zlabel below ...
    accordingly)
242 Scale_y=10;
243
244 %Get the 2-d samples for the "floor"
245 Samples = [w0, E];
246
247 figure; hold on;

```

```

248 %Plot the samples on the "floor"
249 plot3(Samples(:,1),Samples(:,2),zeros(size(Samples,1),1),'k.',
250 'MarkerSize',2)
251
252 %Plot the histograms on the walls from the data in the middle
253 [n_x, xout] = hist(Samples(:,1),30); %creates 30 bars, ...
      n_x=number of elements in each beam, xout=bin limits
254 n_x = n_x ./ ( sum(n_x) *(xout(2)-xout(1)));%Normalizes to ...
      be a pdf
255 [r,r,r,x_Pos,x_Height] = makebars(xout,n_x);%Creates the bar ...
      points
256 plot3(x_Pos, Y(end)*ones(size(x_Pos)),x_Height, '-k')
257
258 %Now plot the other histograms on the wall
259 [n_y, yout] = hist(Samples(:,2),20);
260 n_y = n_y ./ ( sum(n_y) *(yout(2)-yout(1)));
261 [r,r,r,y_Pos,y_Height] = makebars(yout,n_y);
262 plot3(X(1)*ones(size(y_Pos)),y_Pos, Scale_y*y_Height, '-k')
263
264 %Now plot the 1-d pdfs over the histograms
265 plot3(X, ones(size(X))*Y(end), Z_x, '-r', 'LineWidth',2);
266 plot3(ones(size(Y))*X(1), Y, Scale_y*Z_y, '-b', 'LineWidth',2);
267
268 %Make the figure look nice
269 grid on; view(45,55);
270 xlabel('w_0 (mm)'), ylabel('E (GPa)'),zlabel('p w_0(.), 10*p ...
      E(.)')
271 axis([X(1) X(end) Y(1) Y(end)])
272 title('Latin hypercube sampling')
273
274 %-----sy, E scatter with ...
      distributions-----
275 %Define limits of plotting
276 X = min(sy)-1*std(sy):0.1:max(sy)+1*std(sy);
277 Y = mean(E)-4*std(E):1:mean(E)+4*std(E);
278
279 %2-d Mean and St.dev. matrix
280 MeanVec = [mean(sy) mean(E)];
281 StdVec= [std(sy),std(E)];
282
283 %Get the 1-d PDFs for the "walls"
284 Z_x = ...
      lognpdf(X,log(MeanVec(1)^2/sqrt(MeanVec(1)^2+StdVec(1)^2)),
285 sqrt(log(1+(StdVec(1)/MeanVec(1))^2)));
286 Z_y = normpdf(Y,MeanVec(2),StdVec(2));
287
288 %Scale the y-axis pdf(then modify xlabel below accordingly)
289 Scale_y=0.5;
290
291 %Get the 2-d samples for the "floor"
292 Samples = [sy, E];
293
294 figure; hold on;
295 %Plot the samples on the "floor"
296 plot3(Samples(:,1),Samples(:,2),zeros(size(Samples,1),1),'k.',
297 'MarkerSize',2)
298

```

```

299 %Plot the histograms on the walls from the data in the middle
300 [n_x, xout] = hist(Samples(:,1),20); %creates 20 bars, ...
      n_x=number of elements in each beam, xout=bin limits
301 n_x = n_x ./ ( sum(n_x) * (xout(2)-xout(1))); %Normalizes to ...
      be a pdf
302 [x_pos, x_Height] = makebars(xout, n_x); %Creates the bar ...
      points
303 plot3(x_Pos, Y(end)*ones(size(x_Pos)), x_Height, '-k')
304
305 %Now plot the other histograms on the wall
306 [n_y, yout] = hist(Samples(:,2),20);
307 n_y = n_y ./ ( sum(n_y) * (yout(2)-yout(1)));
308 [y_Pos, y_Height] = makebars(yout, n_y);
309 plot3(X(1)*ones(size(y_Pos)), y_Pos, Scale_y*y_Height, '-k')
310
311 %Now plot the 1-d pdfs over the histograms
312 plot3(X, ones(size(X))*Y(end), Z_x, '-r', 'LineWidth',2);
313 plot3(ones(size(Y))*X(1), Y, Scale_y*Z_y, '-b', 'LineWidth',2);
314
315 %Make the figure look nice
316 grid on; view(45,55);
317 xlabel('s_y(mm)'), ylabel('E(GPa)'), zlabel('2*p s_y(.), p E(.)')
318 axis([X(1) X(end) Y(1) Y(end)])
319 title('Latin hypercube sampling')
320
321
322 %-----Bivariate 3D ...
      histograms-----
323 figure
324 hist3([w0 sy], 'Nbins', [40 ...
      40], 'CDataMode', 'auto', 'FaceColor', 'interp')
325 xlabel('w_o(mm)'), ylabel('s_y(MPa)'), zlabel('No of Samples')
326 colorbar
327
328 figure
329 hist3([w0 E], 'Nbins', [40 ...
      40], 'CDataMode', 'auto', 'FaceColor', 'interp')
330 xlabel('w_o(mm)'), ylabel('E(GPa)'), zlabel('No of Samples')
331 colorbar
332
333 figure
334 hist3([E sy], 'Nbins', [40 ...
      40], 'CDataMode', 'auto', 'FaceColor', 'interp')
335 xlabel('E(GPa)'), ylabel('s_y(MPa)'), zlabel('No of Samples')
336 colorbar

```





## Appendix B

# Anslys Source Code

```

!*****
!* The following script is used in APDL v17.0 and receives as input two *
!* matrices. The first N1x4 matrix contains the statistical variables *
!* w0,sy,E and the applied displacement dl. The second is a N2x2 matrix *
!* containing the plate scantlings b and t. Then, two sequential loops *
!* are operated in order to calculate the reaction force over time. *
!* The resulting .txt file contains the maximum reaction force fx. *
!*****

/CLEAR

!=====
! IMPORTING DATA FROM .TXT FILE
!=====

!First matrix containing w0,sy,E
/INQUIRE,numlines,LINES,'Cube_Points','txt'

*DEL,mytable,,NOPR
*DIM,mytable,TABLE,numlines-1,3
*TREAD,mytable,'Cube_Points','txt',,to_skip

*DEL,myarray,,NOPR
*DIM,myarray,ARRAY,numlines,4

*vfun,myarray(1,1),copy,mytable(0,0) ! Shift down and right
*vfun,myarray(1,2),copy,mytable(0,1) ! Shift down and right
*vfun,myarray(1,3),copy,mytable(0,2) ! Shift down and right
*vfun,myarray(1,4),copy,mytable(0,3) ! Shift down and right

!Second matrix containing b,t
/INQUIRE,numlines2,LINES,'Dimensions','txt'

*DEL,mytable2,,NOPR
*DIM,mytable2,TABLE,numlines2
*TREAD,mytable2,'Dimensions','txt',,to_skip

*DEL,myarray2,,NOPR
*DIM,myarray2,ARRAY,numlines2,2

```

```

*vfun,myarray2(1,1),copy,mytable2(1,0) ! Shift column to right
*vfun,myarray2(1,2),copy,mytable2(1,1) ! Shift column to right

!=====
!~~~~~ LOOP START ~~~~~
!=====

*DO,QQ,1,numlines2

!Saves file to this point so it can reload while keeping parameters
SAVE,'FINAL','db','C:\Users\stefa\'

*DO,ZZ,1,numlines

w0=myarray(ZZ,1,1) !mm
sy=myarray(ZZ,2,1) !MPa
E=myarray(ZZ,3,1) !MPa

!=====
! INSERT PLATE SCANTLINGS
!=====

a=3850 !mm
b=myarray2(QQ,1,1) !mm
t=myarray2(QQ,2,1) !mm
v=0.3 !Poisson's Ratio

!Parameters to change
Et=1000 !Tangent Modulus
ES=50 !Element Size
dl=myarray(ZZ,4,1) !Applied Displacement

!=====
! BUCKLING HALF WAVE CALCULATION
!=====

n_plate=1
*DO,JJ,1,1000
*IF,(n_plate**2+n_plate)**(0.5),LE,a/b,THEN
n_plate=n_plate+1
*ELSEIF,(n_plate**2+n_plate)**(0.5),GE,a/b,THEN
*EXIT
*ENDIF
*ENDDO
n_plate=ABS(n_plate)

```

```
!=====
! ELEMENT TYPE
!=====

/PREP7

!Very important. The solution doesn't converge well with SHELL181
ET,1,SHELL281
MPTEMP,,,,,,,,
MPTEMP,1,0
MPDATA,EX,1,,E
MPDATA,PRXY,1,,v

!=====
! SECTION DEFINITION
!=====

SECTYPE,1,SHELL,,plate
SECDATA,t,1,0.0,5! thickness, material, angle, integration points
SECOFFSET,MID

!=====
! PLATE DESIGN
!=====

!Keypoints
K,1,0,0,,
K,2,a,0,,
K,3,a,b,,
K,4,0,b,,

!Create plate area with skinning
LSTR,1,2
LSTR,3,4
ASKIN,1,2

!Assign mesh attributes to the plate
ASEL,S,,1
AATT,1,,,1
ESIZE,ES
AMESH,1

!!!!
ALLSEL,ALL
APLOT,ALL
```

```

NUMMRG,ALL, , , ,LOW

!Detach mesh in order to modify nodes
MODMSH,DETACH

!=====
! LOCAL PLATE BUCKLING
!=====

CSYS,0
NSEL,S,LOC,Y,0,b

*GET,NNUMBER,NODE,0,NUM,MAX!FIND MAXIMUM NODE IN FOR *DOLOOP
PI=4*ATAN(1)

*DO,II,1,NNUMBER
*IF,NSEL(II),EQ,1,THEN
*GET,TMPX,NODE,II,LOC,X
*GET,TMPY,NODE,II,LOC,Y
*GET,TMPZ,NODE,II,LOC,Z
Z_PLATE=w0*SIN(n_plate*PI*TMPX/a)*SIN(PI*TMPY/b)
NMODIF,II,TMPX,TMPY,TMPZ+Z_PLATE
*ENDIF
*ENDDO

!=====
! MATERIAL PROPERTIES
!=====

/PREP7
TB,BISO,1,1,2,
TBTEMP,0
TBDATA,,sy,Et,,,,
ERESX,NO
FINISH

!=====
! COUPLING
!=====

/PREP7
NSEL,S,LOC,x,0
CP,1,UX,ALL

```

```
!=====
! SOLUTION
!=====

/SOLU
CSYS,0
ANTYPE,STATIC
AUTOTS,1
NLGEOM,1
NSUBST,300,500,200
OUTRES,ERASE
OUTRES,ALL,ALL

!Select nodes at periphery
NSEL,S,LOC,y,0
NSEL,A,LOC,y,b
NSEL,A,LOC,x,0
NSEL,A,LOC,x,a
D,ALL,UZ,0

!Select nodes at X=a
NSEL,S,LOC,x,a
D,ALL,UX,0

!Select nodes at X=0, Y=0
NSEL,S,NODE, ,1
D,ALL,UY,0
D,ALL,ROTZ,0

!Apply deformation at X=0
NSEL,S,LOC,x,0
D,ALL,UX,d1

!=====
! SOLUTION CALCULATION
!=====

ALLSEL, ALL
/STATUS,SOLU
SOLVE

FINISH

!=====
! EXPORTING RESULTS
!=====

/POST1
```

```

CSYS,0
SET, LAST
ALLSEL
*GET, SB, ACTIVE, 0, SET, SBST
*CFOPEN, Reaction_Forces_FX, txt, , APPEND

fxmax=1
*DO, I, 1, SB
SET, 1, I
*GET, fx, NODE, 1, RF, FX
*IF, fx, GT, fxmax, THEN
fxmax=fx
*ENDIF
*ENDDO

!Checking if the S-S curve has reached sult
SET, 1, SB
*GET, fx, NODE, 1, RF, FX
fxlast=fx

*IF, fxlast, LT, fxmax, THEN
*VWRITE, fxmax
(E16.8)
*CFCLOSE
*ELSE
*VWRITE, fxmax, 0
(E16.8, E16.8)
*CFCLOSE
*ENDIF

FINISH

RESUME, 'FINAL', 'db', 'C:\Users\stefa\'', 0, 0

*ENDDO !End of ZZ loop

!-----
!Adds a new empty line for every scantlings set
*CFOPEN, Reaction_Forces_FX, txt, , APPEND
*VWRITE,
()
*CFCLOSE
!-----

*ENDDO !End of QQ loop
!=====
!~~~~~ LOOP END ~~~~~
!=====

```